Swayless Point-to-Point Positioning of an Overhead Crane

Lassi Väinölä

School of Electrical Engineering

Thesis submitted for examination for the degree of Master of Science in Technology.

Espoo 14.3.2016

Thesis supervisor:

Prof. Marko Hinkkanen

Thesis advisor:

M.Sc. Mikko Norrkniivilä

Aalto University
School of Electrical
Engineering

AALTO UNIVERSITY
SCHOOL OF ELECTRICAL ENGINEERING

ABSTRACT OF THE
MASTER'S THESIS

Author: Lassi Väinölä

Title: Swayless Point-to-Point Positioning of an Overhead Crane

Date: 14.3.2016 Language: English Number of pages: 9+59

Department of Electrical Engineering and Automation

Professorship: Electrical Drives

Supervisor: Prof. Marko Hinkkanen

Advisor: M.Sc. Mikko Norrkniivilä

In overhead cranes, a payload tends to oscillate from movements of a trolley. Oscillations cause safety issues and make positioning of the load difficult. Moreover, waiting for swaying to damp takes time, thus also reducing productivity. The aim of this thesis was to develop an algorithm which enables swayless point-to-point positioning of a crane. This thesis studies pre-computed and real-time command shaping methods which allow acceleration of the trolley to given movement speed without swaying of the payload. Investigated real-time command shapers used input shaping. Positioning algorithms were tested and compared using Simulink simulations. Test cases included point-to-point positioning with correct and incorrect system parameters, a variable position reference and positioning during hoisting. Results showed that a zero vibration and derivative (ZVD) shaper performed the best. Performance of the ZVD shaper was also tested using a real crane. As the result of the tests, the ZVD shaper can remove payload swaying and enables positioning with ease. The ZVD shaper can be used for a both speed and position shaping.

Keywords: anti-sway, input shaping, overhead crane, positioning

AALTO-YLIOPISTO
SÄHKÖTEKNIIKAN KORKEAKOULU

DIPLOMITYÖN
TIIVISTELMÄ

Tekijä: Lassi Väinölä

Työn nimi: Siltanosturin heilahdukseton paikoitus

Päivämäärä: 14.3.2016 Kieli: Englanti Sivumäärä: 9+59

Sähkötekniikan ja automaation laitos

Professuuri: Sähkökäytöt

Työn valvoja: Prof. Marko Hinkkanen

Työn ohjaaja: DI Mikko Norrkniivilä

Siltanostureissa vaunun liikuttaminen aiheuttaa kuorman heilumista. Kuorman heilunta on turvallisuusriski ja se vaikeuttaa merkittävästi kuorman paikoittamista. Lisäksi heilunnan vaimeneminen vie aikaa, mikä heikentää tuottavuutta. Työn tavoitteena oli kehittää algoritmi, joka mahdollistaa siltanosturin heilahduksettoman paikoituksen. Tässä työssä tarkasteltiin esilaskettuja liikeprofiileita sekä reaaliaikaista ohjearvon muokkausta, mitkä mahdollistavat nosturien vaunun kiihdyttämisen annettuun nopeuteen ilman että kuorma jää heilumaan. Paikoitusalgoritmeja testattiin ja vertailtiin Simulink-simulaatioiden avulla. Testitilanteissa testattiin paikoitusta oikeilla ja väärillä järjestelmäparametreilla, paikkaohjeen muuttumista ja paikoitusta köyden pituuden muuttuessa. Simulointitestien perusteella ”zero vibration and derivative” -suodatin (ZVD) todettiin parhaimmaksi menetelmäksi. ZVD-suodatinta testattiin myös oikealla nosturilla. Testitulosten perusteella ZVD-suodatin pystyy poistamaan kuorman heilunnan ja mahdollistaa helpon paikoituksen. ZVD-suodatinta voidaan käyttää sekä nopeus- että paikkaohjeen muokkaamiseen.

Avainsanat: heilunnanesto, ohjearvon muokkaus, paikoitus, siltanosturi

Preface

This master's thesis was carried out at ABB Oy. I am grateful for my advisor Mikko Norrkniivilä for guidance and regular feedback during my thesis. I would also like to thank professor Marko Hinkkanen who supervised this work and gave excellent guidance about scientific writing. Special thanks to Mikael Holmberg, Billy-Tao Zhang and everybody else who aided me during this thesis. Lastly, I would like to express my gratitude for my friends and family for support and encouragement.

Otaniemi, 14.3.2016

Lassi M. Väinölä

Contents

Abstract ii

Abstract (in Finnish) iii

Preface iv

Contents v

Symbols and Abbreviations vii

1 Introduction 1

2 Pre-Computed Command Profile 3
2.1 Equations of Motion . . . 3
2.2 Phase Plane . . . 5
2.3 Acceleration Strategies . . . 6
2.3.1 Constant Acceleration Strategy . . . 7
2.3.2 Limited Acceleration Strategy . . . 7
2.3.3 Minimum Time Strategy . . . 7
2.4 Sway Compensation . . . 10
2.4.1 Sway Compensation Acceleration . . . 13
2.4.2 Speed Providing Acceleration . . . 16

3 Input Shaping 17
3.1 Introduction to Input Shaping . . . 17
3.2 Zero Vibration Shapers . . . 19
3.3 Zero Vibration and Derivative Shapers . . . 21

4 Crane Positioning 25
4.1 Positioning module . . . 25
4.2 Positioning with Pre-Computed Command . . . 25
4.2.1 Minimum Time Strategy . . . 28
4.2.2 Bang-Off-Bang Control . . . 30
4.2.3 Trigonometric Shaping . . . 33
4.3 Positioning with Input Shaping . . . 33

5 Simulations 35
5.1 Implementation of the Simulation Model . . . 35
5.1.1 Positioning module . . . 35
5.2 Simulation Results . . . 38
5.2.1 Point-to-Point Positioning . . . 38
5.2.2 Changing Position Reference . . . 43
5.2.3 Variable Rope Length . . . 43
5.3 Simulations Summary . . . 46

6 Hardware Tests **49**
6.1 Test Setup 49
6.2 Positioning Tests 50

7 Summary **54**

References **55**

A Derivation of ZVD Equations **57**

B Interpolator Code **58**

Symbols and Abbreviations

Symbols

a_{acc}	positioning acceleration
a_{dec}	positioning deceleration
a_c	sway compensation acceleration
$a_{\max}$	maximum acceleration
A_i	amplitude of the impulse i
A_Σ	amplitude of the total vibration after last impulse
$A_\uparrow$	amplitude of the unity-magnitude impulse
b	damping coefficient
B_i	$\frac{A_i\omega_n}{\sqrt{1-\xi^2}}e^{-\xi\omega_n(t-t_i)}$
$C(\omega_n,\xi)$	sum of cosine coefficients in $V(\omega_n,\xi)$
E_k	kinetic energy of the system
$\overrightarrow{F}$	generalized forces
F_x	horizontal force acting on the trolley
F_θ	viscous damping force acting on the pendulum
g	gravitational acceleration
j	jerk
k_1	direction coefficient in the area 1
k_2	direction coefficient in the area 2
K	$e^{-\frac{\xi\pi}{\sqrt{1-\xi^2}}}$
L	rope length
L_a	actual rope length
L_m	model rope length
$\mathcal{L}$	Lagrangian
m	mass of the payload
M	mass of the trolley
N	number of impulses
N_b	size of the ring buffer
P	represents state of the pendulum in the phase-plane
$\overrightarrow{q}$	generalized displacements
Q	mirror image point
$\overrightarrow{r_T}$	position vector of the trolley
$\overrightarrow{r_L}$	position vector of the payload
R	distance from origin to point P
R_1	radius of the circle drawn by pendulum movement
s	complex number used in Laplace domain
s_{act}	actual position of the trolley
s_{ref}	position reference
s_e	position error
s_s	shaped position reference
s_t	target position

$S(\omega_n, \xi)$	sum of sine coefficients in $V(\omega_n, \xi)$
t_{acc}	duration of acceleration pulse
t_c	duration of the constant speed phase
t_i	time location of the impulse i
t_d	duration of the sway compensation acceleration
t_w	waiting time of the sway compensation acceleration
T_d	damped period of the oscillation
v_{act}	actual speed of the trolley
v_0	initial speed of the trolley when positioning starts
v_{ref}	reference speed
v_{out}	speed reference to speed controller
v_s	shaped speed reference
v_t	travel speed
U	potential energy of the system
$V(\omega_n, \xi)$	percentage residual vibration
x	position of the trolley
z	number of full constant speed cycles in the bang-off-bang control
α	travel time factor
θ	swing angle of the payload
θ_s	scaled swing angle
θ_0	initial angle of the pendulum
$\theta_{\max}$	maximum angle of the pendulum
$\dot{\theta}_s$	scaled angular velocity
$\dot{\theta}_{\max}$	maximum angular velocity
$\dot{\theta}_0$	initial angular velocity of the pendulum
σ	central angle of point P
τ	period of the pendulum
ξ	damping ratio of the system
ξ_a	actual damping ratio
ξ_m	modeling damping ratio
ϕ_i	$\omega_n\sqrt{1-\xi^2}t_i$
φ	angle between R and positive x-axis in the clockwise direction
ψ	$\tan^{-1}\left(\dfrac{\sum_{i=1}^{N} B_i \cos\phi_i}{\sum_{i=1}^{N} B_i \sin\phi_i}\right)$
ω_n	natural frequency of the pendulum
ω_{na}	actual natural frequency
ω_{nm}	modeling natural frequency

Operators

$\frac{\mathrm{d}}{\mathrm{d}t}$	derivative with respect to variable t
$\frac{\partial}{\partial t}$	partial derivative with respect to variable t
$\dot{a}$	derivative of a with respect to time
$\overrightarrow{r}$	vector r
$\lvert a \rvert$	absolute value of a
$\sum_{i=1}^{N}$	sum over index i from 1 to N
$*$	convolution
$\int_a^b f(t)\mathrm{d}t$	definite integral of function f from a to b with respect to variable t

Abbreviations

FIR	finite impulse response
HTL	high transistor logic
IIR	infinite impulse response
PID	proportional-integral-derivative
PLC	programmable logic controller
ZV	zero vibration
ZVD	zero vibration and derivation

1 Introduction

For over a century, overhead cranes have been widely used in many industrial areas, including factories, nuclear power plants and steelworks. Overhead cranes are flexible in nature which leads to one major complication, a payload tends to oscillate when moving the load or as a result of external disturbances (e.g., wind or inadvertent physical disturbances). Oscillations make transportation of loads in a cluttered environment problematic and cause safety risks due to possible collisions. Moreover, accurate positioning of the load becomes more difficult, and waiting for payload oscillations to damp takes time, thus also reducing productivity.

Large oscillations can be caused by a human when operating a speed controlled crane, since the crane follows a given speed reference while using the speed control. Another control approach is to use position control. In the position control mode, the crane moves to a given reference position. Although position control is required for fully-automated cranes, a swaying payload reduces positioning accuracy. As a result, automatic sway controllers, often referred to as "anti-sway" controllers, have been developed to enable faster transfer of a load by eliminating load swing.

An anti-sway system can be implemented with open- and closed-loop control. Closed-loop control has a feedback controller which corrects swaying when it occurs. The difference between the feedback and reference signals is often controlled using proportional-integral-derivative (PID) control. However, sway control relaying on a feedback controller is slow, because the feedback controller is unable to correct any errors until they occur. [1, 2] The feedback can be implemented with sensors though accurate sensing of the sway is often difficult and expensive.

In contrast, open-loop control can anticipate and hence suppress oscillations before they can cause danger to the work environment. Anticipatory suppression of oscillations is possible by modifying a reference command, typically referred to as "command shaping". Command shaping can be categorized into two classes: pre-computed commands and real-time shaping. [3] Cranes are often controlled using one type of real-time command shaping method, which is generally referred to as "input shaping".

An adequate approach to solve the problem of swaying payload during positioning should be able to deal with both accurate positioning and sway control. Traditional methods have solved this problem by combining feedback with input shaping [1, 2]. However, these methods can not be used if position measurement is not available. Moreover, the feedback can lead to instability of the control. Another approach has been to use pre-computed commands, though these are usually limited to only specific conditions. Nevertheless, swayless positioning can be achieved by using pre-computed sinusoidal speed reference [4] or timing acceleration and deceleration phases appropriately [5]. Unfortunately, these methods require that a payload remains at rest in the beginning of the process and that the position reference cannot change midstream. Although input shaping has regularly been combined with feedback to achieve swayless positioning, input shaping has less commonly been used without feedback.

The aim of this thesis is to develop a command shaping algorithm which enables

swayless point-to-point positioning of an overhead crane. The developed algorithm should solve two of three difficulties in crane operation: oscillations induced by commanded motions and accurate positioning. The third difficulty, oscillations induced by external disturbances, cannot be solved with open-loop sway control. Nevertheless, a satisfactory solution can be achieved by implementing two algorithms. The first is for positioning and the second is for sway control. Another approach would be to create a single algorithm which incorporates both positioning and sway control. This thesis compares both pre-computation and real-time input shaping methods in order to determine the most effective algorithm for positioning of the overhead cranes.

The algorithms are tested for the accuracy of point-to-point positioning using Simulink simulations. Positioning algorithms have not been compared in the literature. Robustness of the algorithms is examined using incorrect system parameters, since inaccuracies, such as an incorrect natural frequency, can result in oscillation. Because positioning during hoisting of a payload is the most difficult situation and is often needed to achieve the best productivity, the thesis will also test positioning with changing reference and positioning during hoisting.

Chapter 2 describes crane mechanics, including the principles of pre-computation and sway compensation. Chapter 3 explains the principles underlying the input shaping. Chapter 4 discusses positioning with pre-computed command profile and input shaping. Chapter 5 summarizes simulation results for the algorithms in multiple scenarios. Chapter 6 presents the positioning results from tests performed using a real crane, in which the positioning algorithm used a zero vibration and derivative (ZVD) shaper.

2 Pre-Computed Command Profile

Pre-computed command profiles are calculated at the start of the motion. A reference speed command is given to an anti-sway system which calculates a speed profile which does not cause residual swaying. In a calculated speed profile, accelerations are switched at appropriate times. Pre-computed commands can vary from sharp staircase commands to smoothly changing values. [3]

Pre-computed commands require knowledge about physical model of an overhead crane. In this chapter, the equations of motion for the overhead crane are derived. When the equations of motion are found, pre-computed trolley acceleration strategies are explained by using a phase plane. These accelerations strategies enable acceleration to given speed reference without swaying of a payload. This chapter also explains compensation of an initial swaying.

2.1 Equations of Motion

An overhead crane contains a rigid trolley which can move on fixed rails. The crane can move along a horizontal plane, which are referred to as trolley and long-travel movements. Two-direction motions of the horizontal plane can be divided into two uncoupled one-direction motions. The force F_x used to drive the trolley also causes oscillation of a payload. The payload is suspended from the trolley by a rope, the length of which can be varied with hoisting movement. The payload oscillates around a rope-trolley attachment point and it is treated as one dimensional pendulum with two-degrees-of-freedom sway. For simplification, it is assumed that there are no friction or external disturbances, such as wind. Furthermore, the load acts as a point mass. [6] A model of the overhead crane is shown in Fig. 1.

In Fig. 1 M is the mass of the trolley, L is the length of the rope, m is the mass

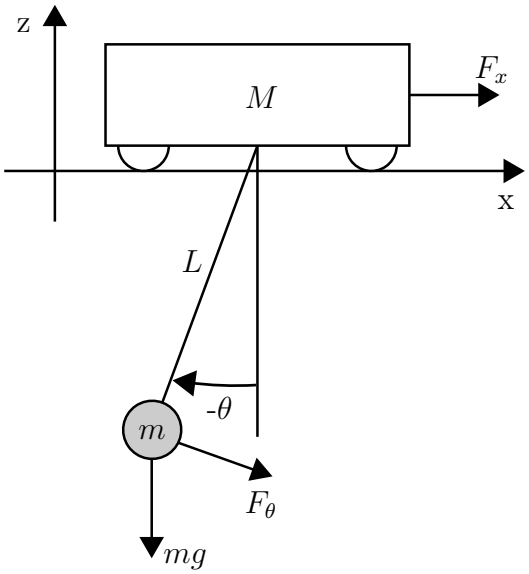

Figure 1: The overhead crane model along one axis.

of the payload, θ is the swing angle of the payload and x is the position of the trolley. The position vectors of the trolley and payload are

$$\overrightarrow{r_T} = \{x, 0\} \tag{1}$$

$$\overrightarrow{r_L} = \{x + L\sin(\theta), -L\cos(\theta)\} \tag{2}$$

The kinetic energy of the system is

$$\begin{aligned} E_k &= \frac{1}{2}m\dot{\overrightarrow{r_L}} \cdot \dot{\overrightarrow{r_L}} + \frac{1}{2}M\dot{\overrightarrow{r_T}} \cdot \dot{\overrightarrow{r_T}} \\ &= \frac{1}{2}m((\dot{x}^2 + \dot{L}\sin(\theta) + L\dot{\theta}\cos(\theta))^2 + (-\dot{L}\cos(\theta) + L\dot{\theta}\sin(\theta))^2) + \frac{1}{2}M\dot{x}^2 \end{aligned} \tag{3}$$

and the potential energy is

$$U = -mgL\cos(\theta) \tag{4}$$

where g is the gravitational acceleration.

The equations of motion can be derived by using Lagrangian mechanics. Lagrangian's equation is defined as follows:

$$\frac{d}{dt}\left(\frac{\partial \mathcal{L}}{\partial \dot{q}_i}\right) - \frac{\partial \mathcal{L}}{\partial q_i} = F_i, \ i = 1, 2 \tag{5}$$

where $\mathcal{L}$ is Lagrangian, $\overrightarrow{q_i}$ is the generalized coordinate and $\overrightarrow{F_i}$ is the corresponding generalized force. Lagrangian is defined as $\mathcal{L} = E_k - U$. Generalized coordinates are conveniently chosen variables which describe the crane system. [7] Let the generalized displacements be $\overrightarrow{q} = \{x, \theta\}$ and corresponding generalized forces are $\overrightarrow{F} = \{F_x, F_\theta\}$. A viscous damping force acting on the pendulum is

$$F_\theta = -bL\dot{\theta} \tag{6}$$

where b is the damping coefficient.

Solving Eq. (5) yields equations of motion:

$$(m + M)\ddot{x} + mL\ddot{\theta}\cos(\theta) + m\dot{L}\dot{\theta}\cos(\theta) - mL\dot{\theta}^2\sin(\theta) = F_x \tag{7}$$

$$mL(L\ddot{\theta} + g\sin(\theta) + 2\dot{L}\dot{\theta} + \ddot{x}\cos(\theta)) = -bL\dot{\theta} \tag{8}$$

Eqs. (7) and (8) do not have analytic solutions. However, a solution can be found, if we assume that swing angles are small and length of the rope is kept constant. Sine and cosine terms are approximated with the first terms of the Taylor polynomial, i.e. $\sin x \approx x$ and $\cos x \approx 1$. An error is less than 1% when $\theta < 14°$. At $\theta = 30°$, the error in the approximation of the sine function is less than 5%. The approximated equations of motion are

$$(m + M)\ddot{x} + mL\ddot{\theta} - mL\dot{\theta}^2\theta = F_x \tag{9}$$

$$\ddot{\theta} + \frac{b}{mL}\dot{\theta} + \frac{g}{L}\theta + \frac{\ddot{x}}{L} = 0 \tag{10}$$

Eq. (10) is a second-order damped oscillatory system. Coefficients can be written as $\frac{b}{mL} = 2\xi\omega_n$, $\frac{g}{L} = \omega_n^2$ and $\frac{1}{L} = \frac{\omega_n^2}{g}$ where ξ is the damping ratio and ω_n is the undamped natural frequency. Using these notations to Eq. (10) yields

$$\ddot{\theta} + 2\xi\omega_n\dot{\theta} + \omega_n^2\theta + \frac{\omega_n^2}{g}\ddot{x} = 0 \tag{11}$$

If the system has damping, the solution uses complex numbers, which makes a time-domain analysis complicated. Overhead cranes exhibit extremely light damping and therefore for pre-computation it is assumed that the damping ratio is zero [8]:

$$\ddot{\theta} + \omega_n^2\theta + \frac{\omega_n^2}{g}\ddot{x} = 0 \tag{12}$$

Eq. (12) is a second-order linear differential equation and general solutions for the swing angle θ and its derivative are

$$\theta(t) = \theta_0\cos(\omega_n t) + \frac{\dot{\theta}_0}{\omega_n}\sin(\omega_n t) + \frac{\ddot{x}}{g}(\cos(\omega_n t) - 1) \tag{13}$$

$$\dot{\theta}(t) = -\theta_0\omega_n\sin(\omega_n t) + \dot{\theta}_0\cos(\omega_n t) - \frac{\ddot{x}\omega_n}{g}\sin(\omega_n t) \tag{14}$$

where θ_0 is the initial angle and $\dot{\theta}_0$ is the initial angular velocity [5, 9]. Period of the pendulum is

$$\tau = 2\pi\sqrt{\frac{L}{g}} \tag{15}$$

The period is derived from the approximated equation, so it is not completely precise and will cause some error to calculations. Maclaurin series for $\sin(\theta)$ gives that error due approximation is of order θ^3 [10].

2.2 Phase Plane

Movement of the pendulum is easier to analyze if the angle and angular velocity are scaled and drawn into a phase plane. In the phase plane x-axis is the angle of the pendulum and y-axis is the angular velocity of the pendulum. Scaled units are achieved by dividing the angle and angular velocity with their maximum values. [11]

The maximum angle θ_{max} is defined as the largest angle that can be reached when the trolley accelerates using the maximum acceleration a_{max} and initial conditions are zero. Eq. (13) is reduced to

$$\theta(t) = -\frac{\ddot{x}}{g} + \frac{\ddot{x}}{g}\cos\left(\sqrt{\frac{g}{L}}t\right) \tag{16}$$

The maximum angle occurs when cosine term is -1. The absolute value of the maximum angle is

$$\theta_{max} = \frac{2a_{max}}{g} \tag{17}$$

The maximum angular velocity is reached when acceleration is stopped at the maximum angle. The total energy of the pendulum varies between kinetic and potential energy. At the stopping moment, there is no angular velocity. The angular velocity of the pendulum is

$$\dot{\theta}(t) = -\theta_0 \omega_n \sin(\omega_n t) \tag{18}$$

The maximum angular velocity can be solved from Eq. (18):

$$\dot{\theta}_{max} = \frac{2a_{max}}{\sqrt{gL}} \tag{19}$$

The scaled angle and speed are

$$\begin{aligned} \theta_s(t) &= \frac{\theta(t)}{\theta_{max}} \\ &= \theta_0 \frac{g}{2a_{max}} \cos(\omega_n t) + \dot{\theta}_0 \frac{\sqrt{gL}}{2a_{max}} \sin(\omega_n t) + \frac{\ddot{x}}{2a_{max}} (\cos(\omega_n t) - 1) \end{aligned} \tag{20}$$

$$\begin{aligned} \dot{\theta}_s(t) &= \frac{\dot{\theta}(t)}{\dot{\theta}_{max}} \\ &= -\theta_0 \frac{g}{2a_{max}} \sin(\omega_n t) + \dot{\theta}_0 \frac{\sqrt{gL}}{2a_{max}} \cos(\omega_n t) - \frac{\ddot{x}}{2a_{max}} \sin(\omega_n t) \end{aligned} \tag{21}$$

Eqs. (20) and (21) can be combined by taking square on both sides and summing the equations together [5]. The result is

$$\left[\theta_s(t) + \frac{\ddot{x}}{2a_{max}}\right]^2 + \left[\dot{\theta}_s(t)\right]^2 = \frac{\theta_0^2 g^2}{4a_{max}^2} + \frac{\theta_0 g \ddot{x}}{2a_{max}^2} + \frac{\ddot{x}^2}{4a_{max}^2} + \frac{\dot{\theta}_0 g L}{4a_{max}^2} \tag{22}$$

Eq. (22) represents the family of circles in the phase plane when acceleration is constant. Centers of the circles are points $\left\{\frac{\ddot{x}}{2a_{max}}, 0\right\}$ and radius of each circle depends on the acceleration and initial conditions. The pendulum moves clockwise in the phase plane and one full circle takes time equal to the period of the pendulum.

2.3 Acceleration Strategies

A crane acceleration profile can be pre-computed by analyzing the phase plane. Following acceleration strategies work when the reference command does not change while the motion is still in progress, the length of the rope stays constant and the damping is assumed to be zero. Presented acceleration strategies neither cause swaying nor remove any existing sway.

When the trolley accelerates, the pendulum follows a non-origin centered circle and during constant speed, the pendulum follows an origin centered circle. The speed refers to the speed of the trolley. Changes in the acceleration cause pendulum to follow a different circle. The easiest solution is to stay whole time on a single circle.

2.3.1 Constant Acceleration Strategy

The simplest way to accelerate a trolley is to use a constant acceleration for a time equal to the period of the pendulum. [12] Fig. 2a shows the movement of the pendulum in the phase plane during the constant acceleration. The drawn circle is in the left half-plane when the trolley accelerates, and in the right half-plane when it decelerates. When the acceleration ends, the pendulum has reached a full circle and returned to the origin. The pendulum always returns to its starting position when an acceleration time is equal to the period of the pendulum. With large periods, this method is too slow. Small periods can also be problematic. With small periods, accelerations are high and the required torque can be higher than the motor can provide. The speed profile and the sway of the pendulum are shown in Fig. 2b. The maximum acceleration $a_{\max}$ is used for scaling the angle and angular velocity.

2.3.2 Limited Acceleration Strategy

When the period of the pendulum is small, high accelerations can be avoided by using limited acceleration strategy. It consists of three acceleration phases which are activated one after another. The first and last accelerations have the same magnitude but the second one has double magnitude [13].

Fig. 3a shows the movement of the pendulum during limited acceleration strategy when acceleration is positive. First the trolley is accelerated for a time $\tau/2$. The pendulum follows the solid line circle during the first phase. After that, begins the second phase and acceleration is doubled. Doubling the acceleration causes the pendulum to stay at a constant position in the phase plane. From Eqs. (20) and (21) can be calculated that the angle stays constant and the angular velocity stays zero. This position can be held as long as needed. If the acceleration during the first and third phases is a and a reference speed is v_{ref}, then a duration of constant angle phase is:

$$t_{\text{const}} = \left| \frac{v_{\text{ref}} - \frac{a\tau}{2}}{a} \right| \tag{23}$$

During the second phase, the pendulum stays at the red point which is the center of the dashed circle. After t_{const}, the trolley is accelerated using the same acceleration as in the first phase for a time $\tau/2$. During the third phase, the pendulum follows the solid line circle. After the third phase, the pendulum reaches the origin.

Limited acceleration strategy is a slow acceleration method and it should only be used with short rope lengths. Fig. 3b shows the speed profile and the sway during limited acceleration strategy.

2.3.3 Minimum Time Strategy

The fastest way to accelerate is to use two acceleration pulses. First the trolley is accelerated to half of the reference speed. Then it moves at a constant speed until time has elapsed to $\tau/2$. Finally, the trolley is accelerated to the reference speed. This method is referred to as minimum time strategy and it enables acceleration in a shorter time than the period of the pendulum. Acceleration phases are identical in

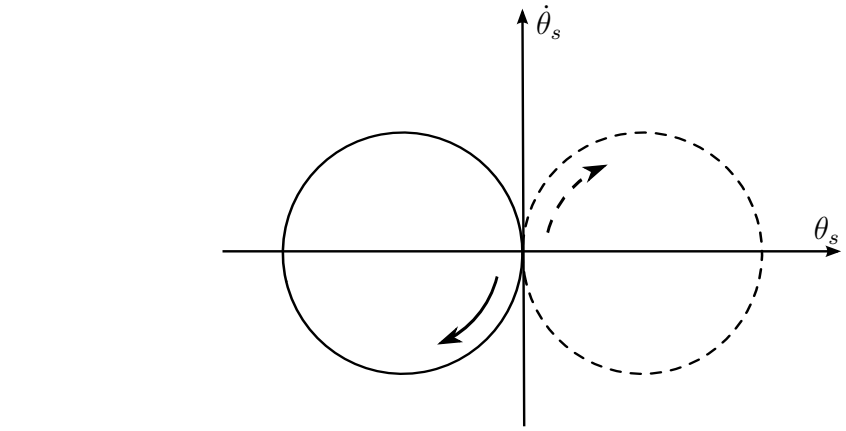

(a) Phase plane

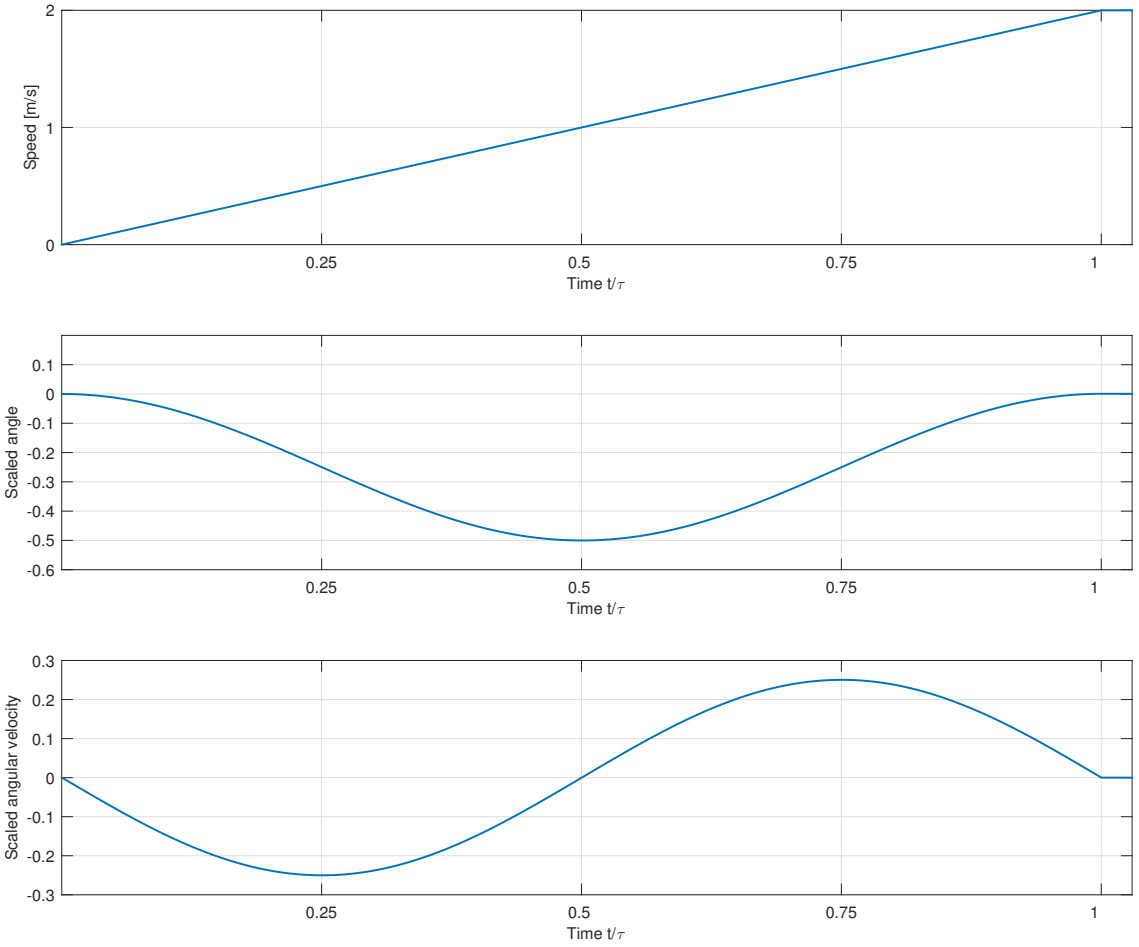

(b) Time domain

Figure 2: The pendulum movement during constant acceleration strategy. (a) The movement in the phase plane. The solid line circle is for positive acceleration and the dashed one for negative. (b) The movement in time domain. In this example, $v_{\text{ref}} = 2$ m/s, $\tau = 7.7695$ s and $a_{\max} = \frac{v_{\text{ref}}}{\tau/2}$. This result is also achieved with the minimum time strategy when $t_{\text{acc}} = \tau/2$.

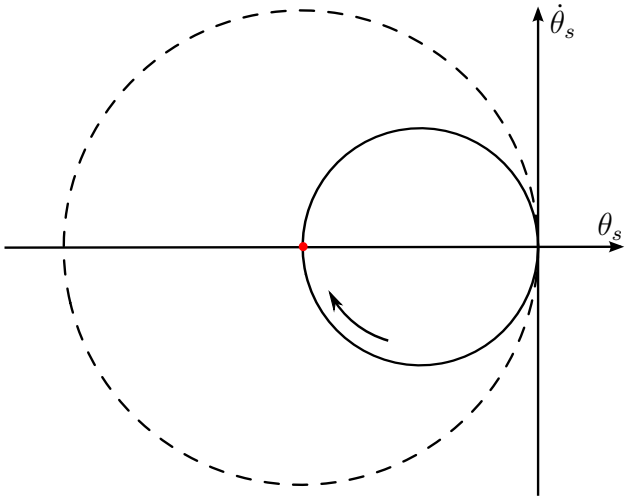

(a) Phase plane

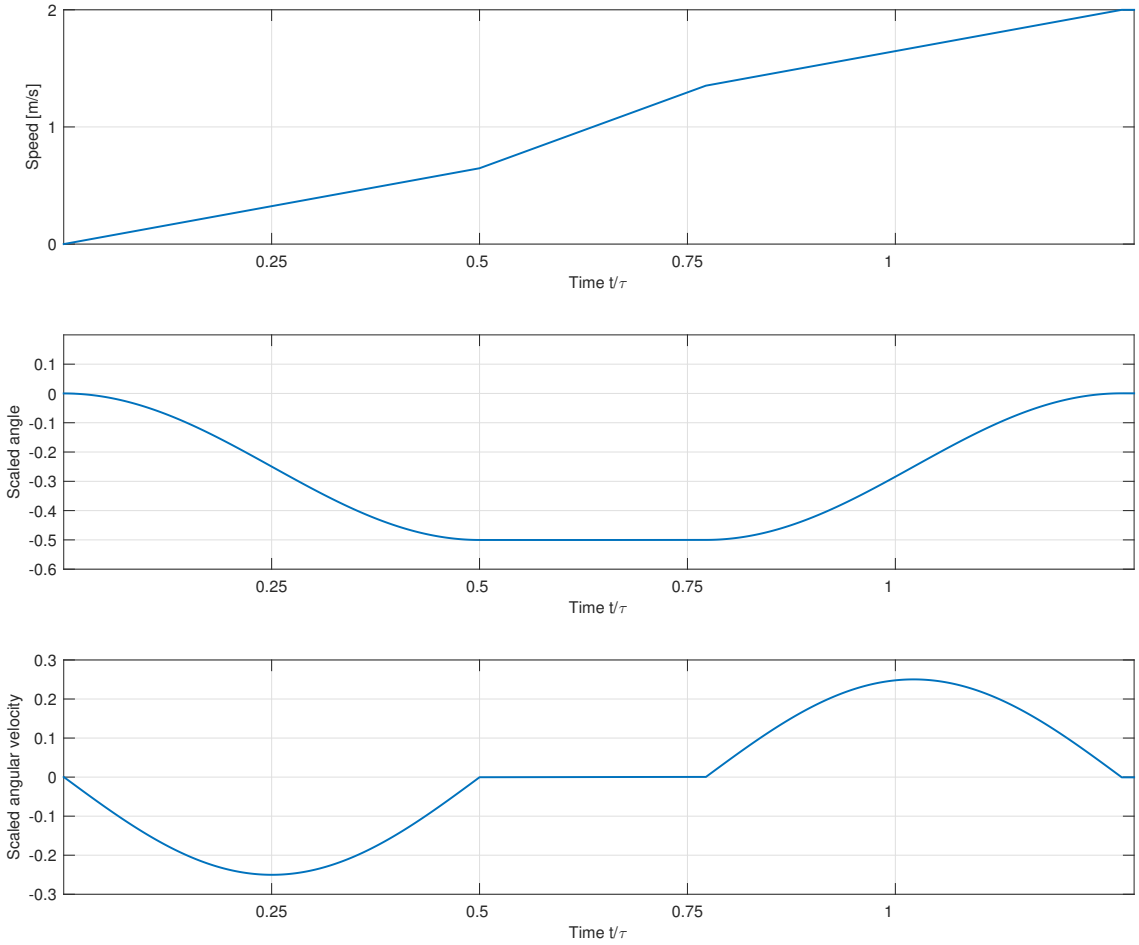

(b) Time domain

Figure 3: The pendulum movement during limited acceleration strategy. (a) The movement in the phase plane. (b) The movement in time domain. In this example, $v_{\text{ref}} = 2$ m/s, $\tau = 7.7695$ s, $t_{\text{acc}} = 6$ s and $a_{\max} = \frac{v_{\text{ref}}}{t_{\text{acc}}}$.

magnitude and duration. There are no limitations on the acceleration duration or magnitude but the second acceleration phase must begin at time $\tau/2$. [12, 14]

Fig. 4a shows the pendulum movement in the phase plane when acceleration is positive and rise time is less than the period. During the first acceleration phase, movement of the pendulum follows the dashed circle. When the speed is half of the reference speed, the acceleration is turned off. Then the movement follows the origin-centered solid line circle. When the time has passed to $\tau/2$, the second acceleration phase begins. The movement switches from the solid line circle to the dashed circle. It is the same circle as during the first acceleration phase. When the speed reference is reached, the acceleration is turned off and the pendulum stays in the origin. The green line shows the path of the pendulum. Fig. 4b shows the speed profile and the sway during minimum time strategy.

Minimum time strategy can produce the same results as constant acceleration and limited acceleration strategies. The produced result depends on the duration of the acceleration phase t_{acc}. If $t_{acc} = \tau/2$, the result is the same as in the constant acceleration strategy. The second acceleration pulse starts right after the first one. If $t_{acc} > \tau/2$, the result is the same as in the limited acceleration strategy. The second acceleration pulse activates before the first one has ended. While both accelerations are on, total acceleration is doubled and the pendulum stays in a constant position. The total rise time is in all cases:

$$t_{\text{tot}} = \frac{\tau}{2} + t_{acc} \tag{24}$$

The only limitation of the minimum time strategy is that when $t_{acc} > \tau/2$, maximum acceleration cannot be used. If both acceleration pulses used maximum acceleration, the total acceleration would be twice the maximum limit during the constant angle phase. This can be prevented by using a smaller acceleration, so that the total acceleration does not exceed the maximum limit while both accelerations are on. Additionally, the maximum acceleration may cause an unwanted jerk which makes smaller accelerations more favorable.

2.4 Sway Compensation

The main disadvantage of pre-computed signals is that reference changes are problematic while current motion is in progress. Either new motion must be delayed until the current motion is completed or the current motion must be interrupted. The pre-computed commands do not leave residual swaying if they are completed. If the pre-computed command is interrupted and a new command is started, there is no certainty that the residual swaying is removed. This problem can be prevented by keeping track of the sway and using additional acceleration which compensates any existing sway. The initial sway is compensated by accelerating the trolley at the right moment.

Pre-computed command shaping is an open-loop control method and the anti-sway system does not have any real information about the swaying of the pendulum. Therefore, the angle and angular velocity of the pendulum are calculated, which is

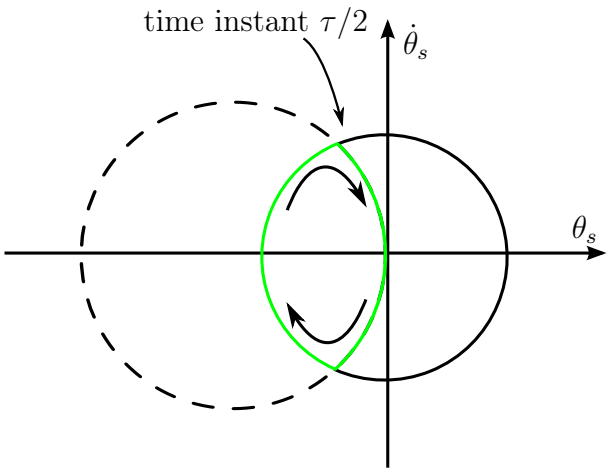

(a) Phase plane

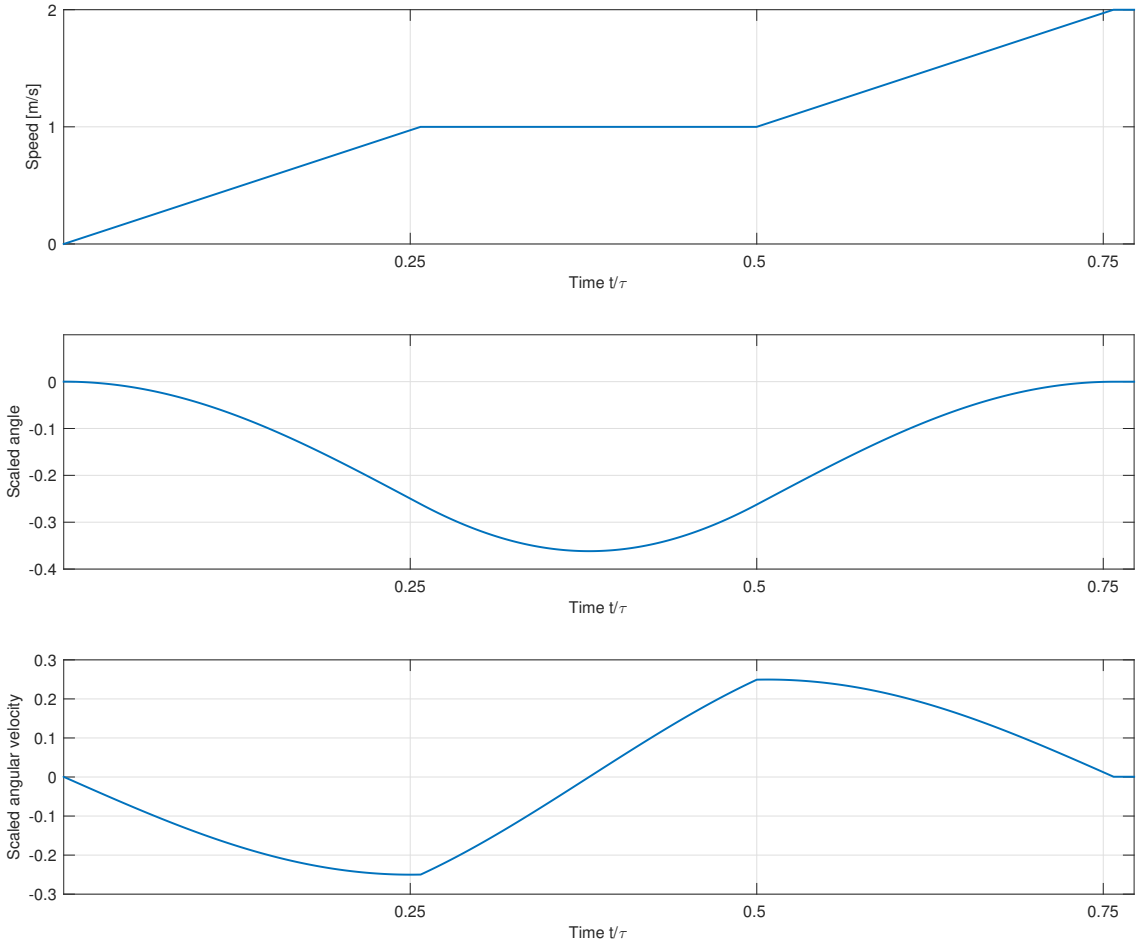

(b) Time domain

Figure 4: The pendulum movement during minimum time strategy. (a) The movement in the phase plane. Path of the pendulum is shown with the green line. (b) The movement in time domain. In this example, $v_{\text{ref}} = 2$ m/s, $\tau = 7.7695$ s, $t_{\text{acc}} = 2$ s and $a_{\max} = \frac{v_{\text{ref}}}{t_{\text{acc}}}$.

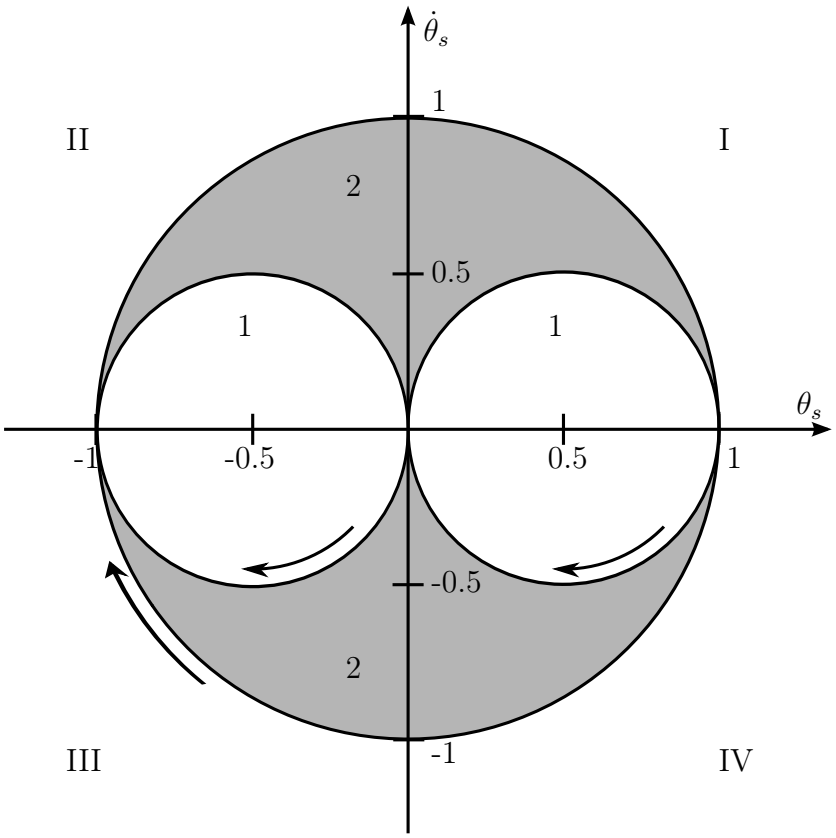

Figure 5: Maximum sized circles drawn by the pendulum movement in the phase-plane.

referred to as sway tracking. The pendulum swaying can be calculated from Eqs. (13) and (14). Another way to track swaying is to numerically integrate Eq. (8) in order to obtain the angular velocity and angle. The latter method is preferable if the rope length varies. When sway tracking is activated, the pendulum should be at rest. Any sway the pendulum has before sway tracking is activated, cannot be removed with the open-loop control.

The pendulum swaying draws circles into a phase plane. Fig. 5 shows maximum sized circles in the phase plane. An area 1 consists of circles drawn by the pendulum when the trolley moves at the maximum acceleration. Positive acceleration draws the left side circle and negative the right side circle. An area 2 is the exterior of the area 1. If the pendulum starts from the origin, circles are drawn inside the area 1 during accelerations. The pendulum can move inside the area 2 if the acceleration is stopped before the pendulum reaches the origin. The main difference between the areas is how long it takes to compensate swaying.

The compensation consists of two parts: a constant speed phase and an acceleration phase. The constant speed phase is not required in second and fourth quadrants of the area 1. Therefore, the acceleration phase begins there immediately.

In the first and third quadrants of the area 1, the pendulum moves at constant speed until it reaches a mirror image point. The mirror image point is a starting

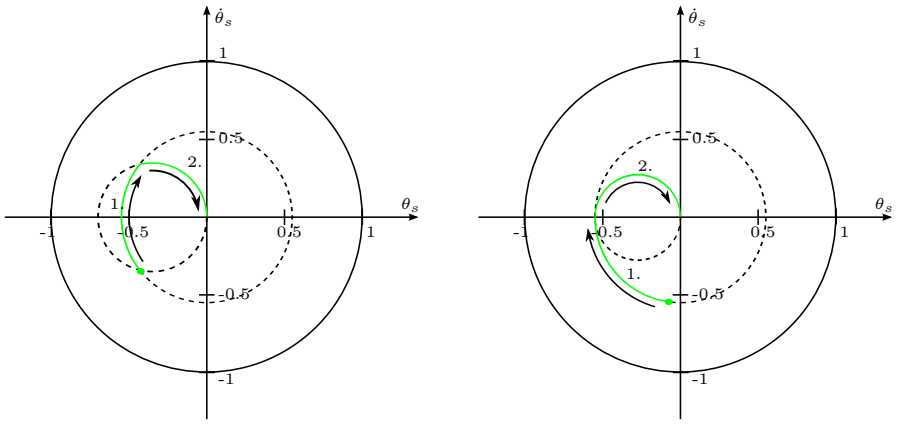

(a) Area 1 (b) Area 2

Figure 6: Sway compensation in the area 1 (a) and area 2 (b). The waiting phase is depicted with 1 and the acceleration phase with 2.

point projected across θ_s-axis. A duration of constant speed phase is referred to as a waiting time. After that the compensation acceleration is turned on and the pendulum is accelerated to the origin. This is portrayed in Fig. 6a where the starting location is the green point. In the second and fourth quadrants, the compensation is done similarly, except the waiting time is zero. The compensation could be also done using a constant acceleration but it is slower than waiting first and then accelerating.

In the area 2, the sway is compensated only when the pendulum is at θ_s-axis, i.e. pendulum's angle is at the maximum. This is shown in Fig. 6b. The only differences are that, in the area 2 acceleration duration is always $\tau/2$ and during waiting time pendulum moves to the θ_s-axis.

2.4.1 Sway Compensation Acceleration

In order to compensate the sway, the sway compensation acceleration and duration of the constant speed and acceleration phases must be calculated. They are calculated from circles in the phase plane. Fig. 7 has two circles: the dashed circle for a constant speed and the solid line circle for an acceleration.

In Fig. 7 point P represents the state of the pendulum and Q is the mirror image point. R is the distance from origin to point P and R_1 is the radius of the acceleration circle. σ is the central angle of point P when the pendulum moves along a circle to the origin in the clockwise direction. φ is the angle between R and positive θ_s-axis in the clockwise direction. Calculating R_1 shows whether the pendulum is in the area 1 or 2. If $R_1 > 0.5$, the pendulum is in the area 2. [11]

R can be calculated by using Pythagoras theorem:

$$R = \sqrt{\dot{\theta}_s + \theta_s} \tag{25}$$

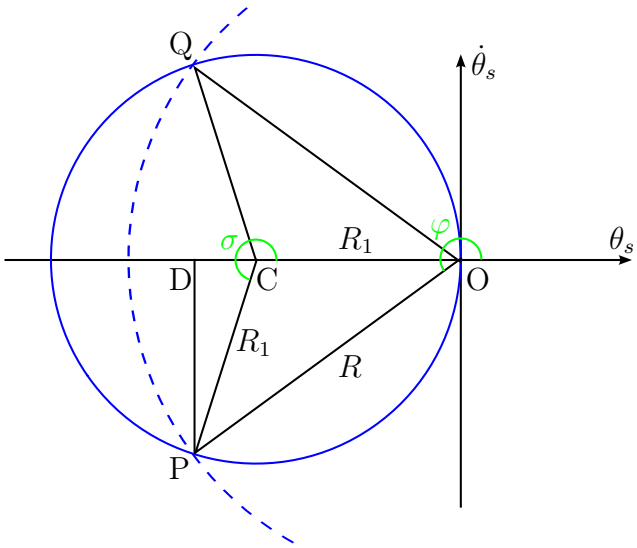

Figure 7: Geometry of the pendulum movement in the phase plane.

The angle φ is calculated by using basic geometry

$$\varphi = \begin{cases} \cos^{-1}\left(\frac{\theta_s}{R}\right) & \text{1st quadrant} \\ \pi - \cos^{-1}\left(\frac{\theta_s}{R}\right) & \text{2nd quadrant} \\ \pi + \cos^{-1}\left(\frac{\theta_s}{R}\right) & \text{3rd quadrant} \\ 2\pi - \cos^{-1}\left(\frac{\theta_s}{R}\right) & \text{4th quadrant} \end{cases} \tag{26}$$

The triangle formed by points OPC is isosceles and the sum of angles of a triangle is always π in Euclidian geometry. This information is used for solving σ:

$$\sigma = \begin{cases} 2\varphi + \pi & 0 \leq \varphi < \frac{\pi}{2} \\ 2\varphi - \pi & \frac{\pi}{2} \leq \varphi < \frac{3\pi}{2} \\ 2\varphi - 3\pi & \frac{3\pi}{2} \leq \varphi < 2\pi \end{cases} \tag{27}$$

The radius R_1 is calculated by using law of sines. In the third quadrant for the triangle PDC applies

$$\frac{R_1}{\sin\left(\frac{\pi}{2}\right)} = \frac{\text{PD}}{\sin(\pi - \sigma)} \tag{28}$$

Using same law for the triangle PDO:

$$\frac{R}{\sin\left(\frac{\pi}{2}\right)} = \frac{\text{PD}}{\sin(\pi - \varphi)} \tag{29}$$

Combining Eqs. (28) and (29) gives us a solution for R_1. Taking the absolute value of the equation makes it valid in all quadrants. The solution for R_1 is

$$R_1 = \begin{cases} \left|\frac{R\sin(\varphi)}{\sin(\sigma)}\right| & \sigma \neq 0,\ \pi \text{ or } 2\pi \\ \frac{R}{2} & \sigma = 0,\ \pi \text{ or } 2\pi \end{cases} \tag{30}$$

The latter case is protection against division by zero, but the result is completely understandable by looking at Fig. 7. If $R_1 < 0.5$, the pendulum is in the area 1. Otherwise the pendulum is in the area 2. A direction of compensation acceleration is determined by a direction coefficient k. It is defined in the area 1 and area 2 as follows

$$k_1 = \begin{cases} 1 & (\theta_s = 0 \wedge \dot{\theta}_s < 0) \vee (\theta_s < 0) \\ -1 & \text{otherwise} \end{cases} \tag{31}$$

$$k_2 = \begin{cases} 1 & (\dot{\theta}_s = 0 \wedge \theta_s < 0) \vee (\dot{\theta}_s < 0) \\ -1 & \text{otherwise} \end{cases} \tag{32}$$

When the trolley moves at the maximum acceleration, the drawn circle is also the largest possible one. When initial conditions are zero, Eq. (22) is reduced to

$$\left[\theta_s(t) + \frac{\ddot{x}}{2a_{max}}\right]^2 + \left[\dot{\theta}_s(t)\right]^2 = \frac{\ddot{x}^2}{4a_{max}^2} \tag{33}$$

From Eq. (33) can be seen that, decreasing the acceleration also decreases the radius of the circle proportionally. Now that the radius of the circle and direction coefficient are known, the compensation acceleration can be calculated as follows

$$a_c = \begin{cases} 2a_{\max} k_1 R_1 & \text{area 1} \\ a_{\max} k_2 R & \text{area 2} \end{cases} \tag{34}$$

The duration of the sway compensation acceleration and the waiting time are also found by using geometry. In the second and fourth quadrants of the area 1 waiting time is not needed but in the first and third quadrants pendulum needs to reach the mirror image point Q. During the waiting time, the pendulum moves along the dashed circle. A time it takes the pendulum to travel a full circle is equal to the period τ. Moving from point P to Q is an arch of the circle and corresponding time is the angle of the arch multiplied with the period. The waiting time in the area 1 is

$$t_{1w} = \begin{cases} \frac{(2\varphi - 2\pi)\tau}{2\pi} & \varphi > \pi \\ 0 & \varphi < \pi \end{cases} \tag{35}$$

The duration of the sway compensation acceleration in the area 1 is the same as it takes to reach point P from the origin, i.e. angle OCP$\cdot\frac{\tau}{2\pi}$. [11] The acceleration is activated at Q and there the movement of the pendulum changes from the dashed circle to the solid line circle. The duration in the area 1 is

$$t_{1d} = \begin{cases} \frac{(2\pi - \sigma)\tau}{2\pi} & \sigma > \pi \\ \frac{\sigma\tau}{2\pi} & \sigma < \pi \end{cases} \tag{36}$$

In the area 2, the waiting time is an arch of full circle:

$$t_{2w} = \begin{cases} \frac{\varphi\tau}{2\pi} & 0 \leq \varphi < \pi \\ \frac{(\varphi - \pi)\tau}{2\pi} & \pi \leq \varphi < 2\pi \\ 0 & \varphi = 2\pi \end{cases} \tag{37}$$

The duration in the area 2 is

$$t_{2d} = \tau \tag{38}$$

Unfortunately, a reference speed usually cannot be reached using the sway compensating acceleration. In addition to sway compensation acceleration, anti-sway system requires another acceleration which produces required speed change. This second acceleration is referred to as speed providing acceleration. [11]

2.4.2 Speed Providing Acceleration

After the sway has been compensated, there is a need for a speed change as the speed of the trolley is not the same as the speed reference. Speed providing acceleration does this required speed change. The required speed change is

$$v_\Delta = v_{\text{ref}} - v_{\text{act}} - a_c t_d \tag{39}$$

where v_{ref} is the speed reference, v_{act} is the actual speed, a_c is the sway compensation acceleration and t_d is the duration of sway compensation acceleration. The speed providing acceleration does not cause any swaying afterwards as it uses acceleration strategies presented in the section 2.3. If a reference command is interrupted, the sway compensation acceleration is activated. On the other hand, speed providing acceleration is always activated when the reference command changes. If the pendulum starts from rest, anti-sway system uses only the speed providing acceleration.

Multiple accelerations can be used simultaneously as the crane model is linearized. Therefore, speed providing acceleration can begin even before the sway has been compensated. Sum of accelerations does not cause swaying if individual accelerations do not cause swaying. The only requirement is that sum of accelerations does not exceed the maximum acceleration. A real crane is not a linear system but an error caused by the linearization is small.

3 Input Shaping

The previous chapter described the principles of pre-computed command shaping. This chapter presents real-time command shaping method called input shaping. The crane model presented in the section 2.1 follows the same transfer function as presented in this chapter.

3.1 Introduction to Input Shaping

A real-time command shaping can be done by filtering the reference command. Filtered responses of the linear systems can be represented with a finite impulse response (FIR) or infinite impulse response (IIR). Input shaping is a variation of FIR filtering. Input shaping is implemented by convolving a reference command with a sequence of impulses. Fig. 8 illustrates how input shaping works. The reference command is a step signal and an input shaper contains two impulses. Convolving a continuous function with a two-impulse sequence consists of three steps:

1. Scale the initial command with the amplitude of the first impulse A_1.
2. Scale the initial command with the amplitude of the second impulse A_2 and shift it to the time location of the second impulse.
3. Add together functions from the steps 1 and 2.

The produced reference is a staircase command with two steps. [15, 16]

Giving a system an impulse will cause the system to vibrate but a second impulse can be applied to the system to cancel vibration induced by the first impulse. Input shapers are designed so that a created command signal tends to cancel its own vibration. [3, 17] Input shaping can eliminate residual vibration but trade-off is larger rise time. Fig. 9 shows a damped second-order system where the second impulse cancels vibration induced by the first impulse. The resultant response is black dotted line and it has zero vibration after the second impulse. [16]

In order to find a input shaper that produces zero vibration at specific frequency, equation for total vibration must be derived. The transfer function of the damped second-order system is

$$G(s) = \frac{\omega_n^2}{s^2 + 2\xi\omega_n s + \omega_n^2} \tag{40}$$

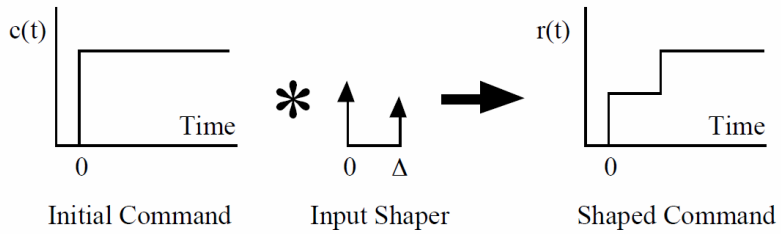

Figure 8: Input shaping a step reference into a staircase. [3]

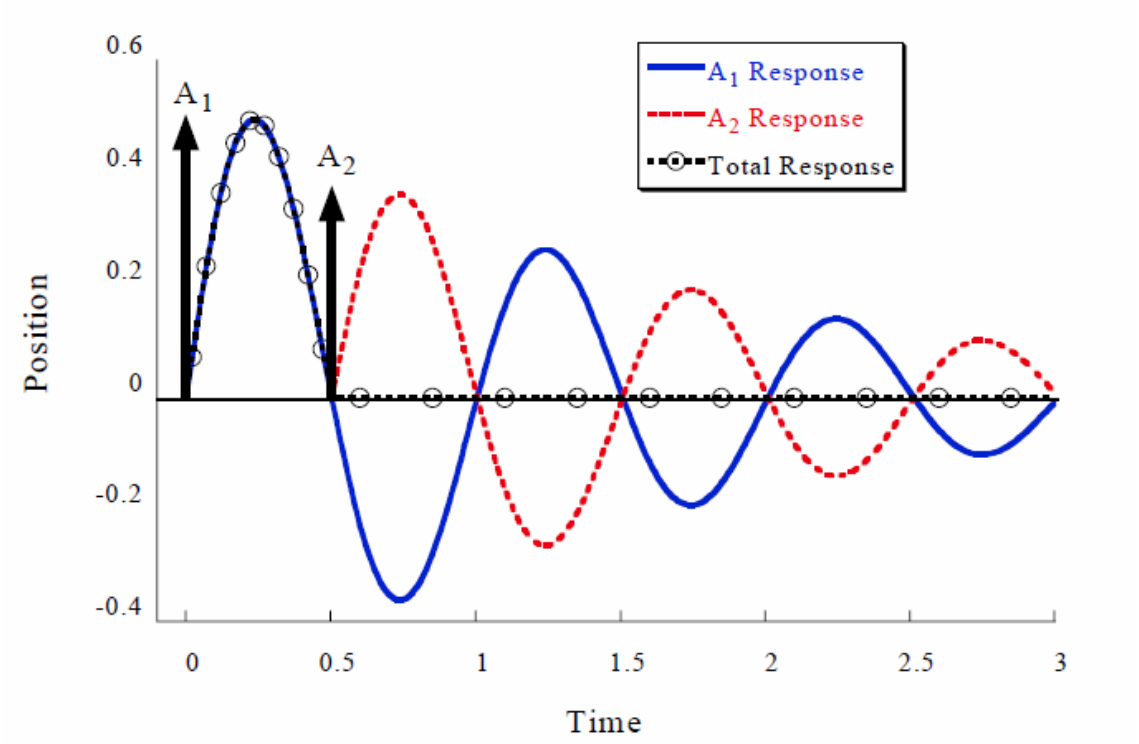

Figure 9: Vibrations caused by impulses and their sum. [16]

where ω_n is the undamped natural frequency of the system, ξ is the damping ratio of the system and s is the complex number used in Laplace domain. The impulse response of the system is

$$y(t) = \left[A \frac{\omega_n}{\sqrt{1-\xi^2}} e^{-\xi\omega_n(t-t_0)} \right] \sin\left(\omega_n \sqrt{1-\xi^2}(t-t_0) \right) \tag{41}$$

where A is the amplitude of the impulse and t_0 is the time of the impulse input. Superposition can be used to find a total response if the system is assumed to be linear and time invariant. The time response to an impulse sequence is

$$y_\Sigma(t) = \sum_{i=1}^{N} \left[A_i \frac{\omega_n}{\sqrt{1-\xi^2}} e^{-\xi\omega_n(t-t_i)} \right] \sin\left(\omega_n \sqrt{1-\xi^2}(t-t_i) \right) \tag{42}$$

Eq. (42) is used for finding the amplitudes of impulses. [16] Fig. 9 shows that superposition of two impulses can be used to cancel a vibration. The same result can be obtained by summing up two impulse responses (both described by Eq. (41)) and expressing the summation for all the times greater than the duration of the input. The result can be reduced by using the following trigonometric identity [18]:

$$B_1 \sin(\omega t + \phi_1) + B_2 \sin(\omega t + \phi_2) = A_\Sigma \sin(\omega t + \psi) \tag{43}$$

where ω is an arbitrary frequency and

$$A_\Sigma = \sqrt{(B_1 \cos\phi_1 + B_2 \cos\phi_2)^2 + (B_1 \sin\phi_1 + B_2 \sin\phi_2)^2}$$
$$\psi = \tan^{-1}\left(\frac{B_1 \cos\phi_1 + B_2 \cos\phi_2}{B_1 \sin\phi_1 + B_2 \sin\phi_2}\right)$$

With N impulses the amplitude of the resultant vibration is

$$A_\Sigma = \sqrt{\left(\sum_{i=1}^{N} B_i \cos\phi_i\right)^2 + \left(\sum_{i=1}^{N} B_i \sin\phi_i\right)^2} \tag{44}$$
$$\phi_i = \omega_n \sqrt{1-\xi^2} t_i$$

The impulses occur at times t_i and the coefficients B_i are found by comparing Eq. (43) to Eq. (42). The coefficients B_i are

$$B_i = \frac{A_i \omega_n}{\sqrt{1-\xi^2}} e^{-\xi\omega_n(t-t_i)} \tag{45}$$

where A_i is the amplitude of ith impulse and t_i is the occurring time of the impulse. The amplitude of the vibration can be scaled by dividing it with a single unity-magnitude impulse's amplitude which is

$$A_\uparrow = \frac{\omega_n}{\sqrt{1-\xi^2}} \tag{46}$$

It is desired that the vibrations are minimized at the time t_N which is time the last impulse occurs. A scaled magnitude of the vibration at the time of the last impulse, i.e. percentage residual vibration, is

$$V(\omega_n, \xi) = e^{-\xi\omega_n t_N} \sqrt{(C(\omega_n, \xi))^2 + (S(\omega_n, \xi))^2} \tag{47}$$

where

$$C(\omega_n, \xi) = \sum_{i=1}^{N} A_i e^{\xi\omega_n t_i} \cos\left(\omega_n \sqrt{1-\xi^2} t_i\right) \tag{48}$$
$$S(\omega_n, \xi) = \sum_{i=1}^{N} A_i e^{\xi\omega_n t_i} \sin\left(\omega_n \sqrt{1-\xi^2} t_i\right) \tag{49}$$

The result leads to zero vibration when Eqs. (48) and (49) are zero. The result is found by solving the impulse amplitudes A_i and impulses' time locations t_i. The simplest input shaper is the zero vibration shaper (ZV). [16, 18]

3.2 Zero Vibration Shapers

A zero vibration shaper produces a command which leads to zero residual vibration at a modeling frequency in minimal time. The residual vibration is only zero when

the model is perfect. The impulses and time locations of these impulses of the ZV shaper are solved by setting Eq. (47) to zero. The solution requires some constraints to prevent zero-valued or infinitely-valued impulses. Sum of all impulses must be equal to one [16, 19]:

$$\sum A_i = 1 \tag{50}$$

With this constraint, the shaped command yields the same final set point as the original command. This single constraint is not sufficient because impulses could take infinitely large positive and negative values. A bounded solution is achieved by limiting the impulses to only positive values [19]:

$$A_i > 0, \quad i = 1, 2, \ldots, N \tag{51}$$

A two-impulse sequence is the simplest way to obtain zero vibration, as can be seen in Fig. 9. This problem has four unknown variables: amplitudes A_1 and A_2 and their time locations t_1 and t_2. The time location of the first impulse can be set to zero, i.e. $t_1 = 0$. The total vibration V is zero when both Eqs. (48) and (49) are zero. Therefore the impulses must satisfy

$$A_1 + A_2 e^{\xi\omega_n t_2} \cos\left(\omega_n \sqrt{1-\xi^2}\, t_2\right) = 0 \tag{52}$$

$$A_2 e^{\xi\omega_n t_2} \sin\left(\omega_n \sqrt{1-\xi^2}\, t_2\right) = 0 \tag{53}$$

Eq. (53) is true when the sine term equals to zero. This occurs periodically

$$\omega_n \sqrt{1-\xi^2}\, t_2 = n\pi \quad n = 1, 2, \ldots \tag{54}$$

The time t_2 can be solved from Eq. (54):

$$t_2 = \frac{n\tau}{2\sqrt{1-\xi^2}} \quad n = 1, 2, \ldots \tag{55}$$

where τ is a period of the pendulum. Because of the periodic nature of the sine function, there are an infinite number of solutions. The shortest time is attained by choosing the smallest value for t_2

$$t_2 = \frac{T_d}{2} \tag{56}$$

where $T_d = \frac{2\pi}{\omega_n \sqrt{1-\xi^2}}$ is the damped period of the oscillation. Eq. (50) is reduced to

$$A_1 + A_2 = 1 \tag{57}$$

A_1 is solved by substituting Eqs. (56) and (57) into (52):

$$A_1 = \frac{e^{\frac{\xi\pi}{\sqrt{1-\xi^2}}}}{1 + e^{\frac{\xi\pi}{\sqrt{1-\xi^2}}}} \tag{58}$$

The equations can be simplified by defining $K = e^{-\frac{\xi\pi}{\sqrt{1-\xi^2}}}$. Zero vibration solution for the two-impulse sequence is following [16, 19]:

$$\begin{bmatrix} A_1 & A_2 \\ t_1 & t_2 \end{bmatrix} = \begin{bmatrix} \frac{1}{1+K} & \frac{K}{1+K} \\ 0 & 0.5T_d \end{bmatrix} \tag{59}$$

When the damping ratio ξ is assumed to zero, Eq. (59) reduces to:

$$\begin{bmatrix} A_1 & A_2 \\ t_1 & t_2 \end{bmatrix} = \begin{bmatrix} \frac{1}{2} & \frac{1}{2} \\ 0 & 0.5\tau \end{bmatrix} \tag{60}$$

The solution causes the same results as the minimum time strategy which was explained in the section 2.3. The main difference is that the ZV shaper will not need additional sway compensation acceleration if the reference changes while a motion is in progress. The main problem with the ZV shaper as well with the pre-computed command shaping is robustness. If there are errors in the system parameters (ω_n and ξ), the result will not lead to zero vibration. [19]

Fig. 10 shows a sensitivity curve for the ZV shaper. The horizontal axis is a normalized frequency which represents a ratio between an actual natural frequency ω_{na} and the modeling frequency ω_{nm}. Vertical axis is percentage residual vibration given by Eq. (47). The residual vibration increases quickly as the deviation between the actual and modeling frequencies increases. However, the sensitivity curve reaches a zero at every odd integer at the x-axis and the ZV shaper never increases vibration, which is demonstrated in Fig. 11. A non-dimensional robustness measure is called the shaper's insensitivity and it is measured by determining the width of the curve at some low level of vibration. For the ZV shaper, 5% insensitivity is 0.06 which means that shaper can keep residual vibration under 5% level when frequency changes $\pm$ 3% . [16, 19]

3.3 Zero Vibration and Derivative Shapers

Robustness of a shaper can be increased with additional constraints. One possibility is to set derivative of (47), with respect to frequency ω_n, equal to zero:

$$\frac{\partial}{\partial\omega_n} V(\omega_n, \xi) = 0 \tag{61}$$

A shaper that satisfies this constraint is called zero vibration and derivative (ZVD) shaper. [16]

Due to Eq. (61) two new equations are added to the system [18]:

$$\frac{\partial}{\partial\omega_n} C = \frac{\partial}{\partial\omega_n} \sum_{i=1}^{N} A_i e^{\xi\omega_n t_i} \cos\left(\omega_n\sqrt{1-\xi^2}t_i\right) = 0 \tag{62}$$

$$\frac{\partial}{\partial\omega_n} S = \frac{\partial}{\partial\omega_n} \sum_{i=1}^{N} A_i e^{\xi\omega_n t_i} \sin\left(\omega_n\sqrt{1-\xi^2}t_i\right) = 0 \tag{63}$$

The result requires three impulses and two more unknowns (A_3 and t_3). Derivation of the result is long and it is given in the appendix A. The times and magnitudes of the ZVD shaper are [16]

$$\begin{bmatrix} A_1 & A_2 & A_3 \\ t_1 & t_2 & t_3 \end{bmatrix} = \begin{bmatrix} \frac{1}{1+2K+K^2} & \frac{2K}{1+2K+K^2} & \frac{K^2}{1+2K+K^2} \\ 0 & 0.5T_d & T_d \end{bmatrix} \tag{64}$$

Fig. 12 shows a sensitivity curve for the ZVD shaper. The ZVD shaper is substantially robuster than the ZV shaper. For the ZVD shaper, 5% insensitivity is 0.286 which is almost 5 times more than the insensitivity of the ZV shaper. Increasing robustness has one drawback: it also increases rise time. Shaped commands have increased rise time duration compared to a non-shaped command. A delay duration of the ZV shaper is half the period of the pendulum while the ZVD shaper has a delay of the period of the pendulum. [3, 19] Robustness can be increased even further by deriving (47) two or three times when solving amplitudes and their time locations. Each derivation also increases the rise time. [20]

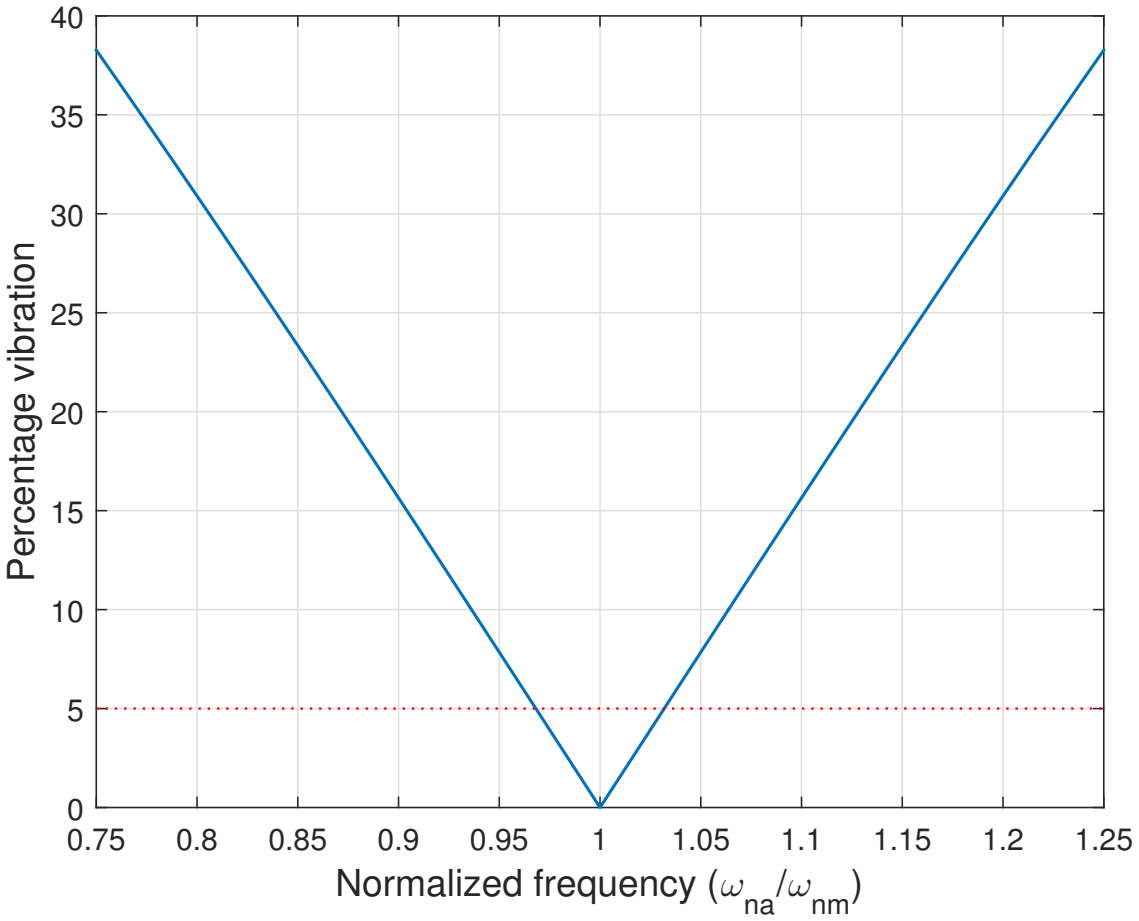

Figure 10: Sensitivity curve for a ZV shaper. ω_{na} is the actual natural frequency and ω_{nm} is the modeling frequency.

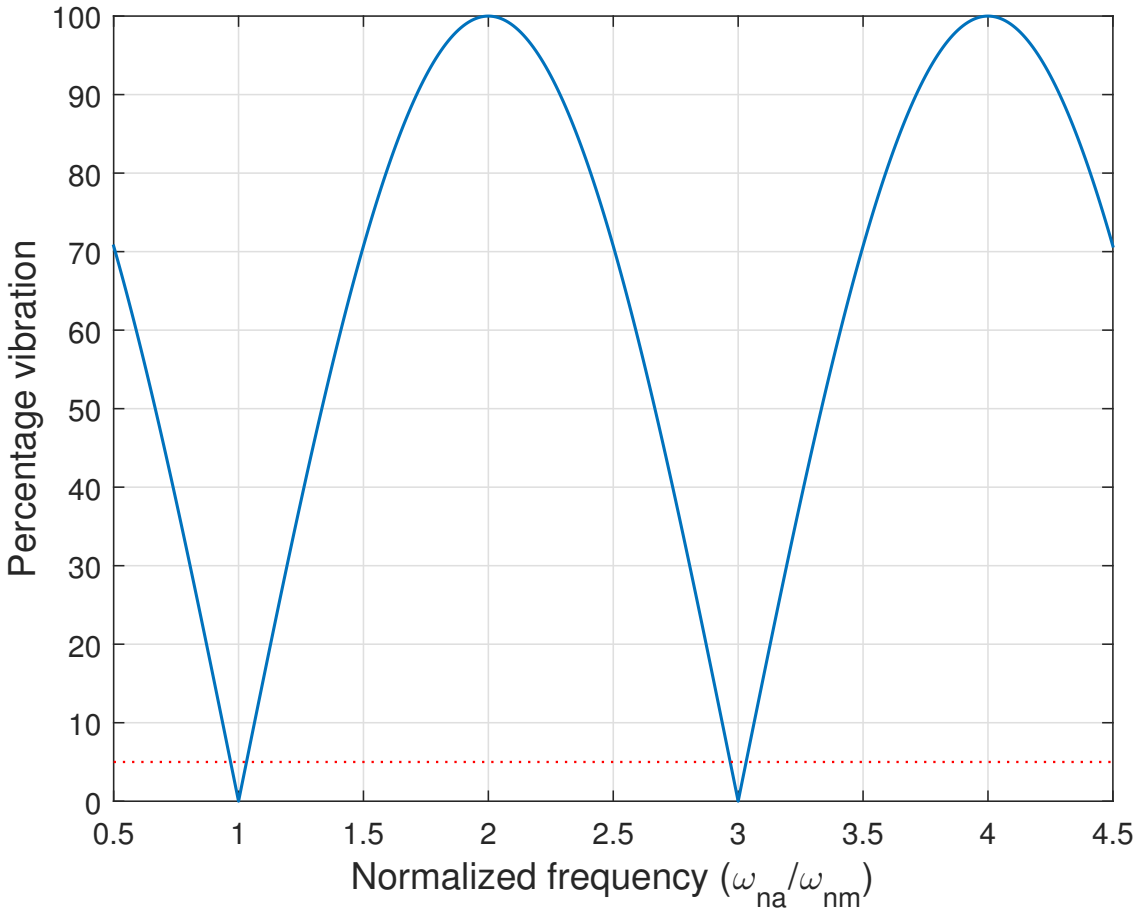

Figure 11: Extended sensitivity curve for a ZV shaper.

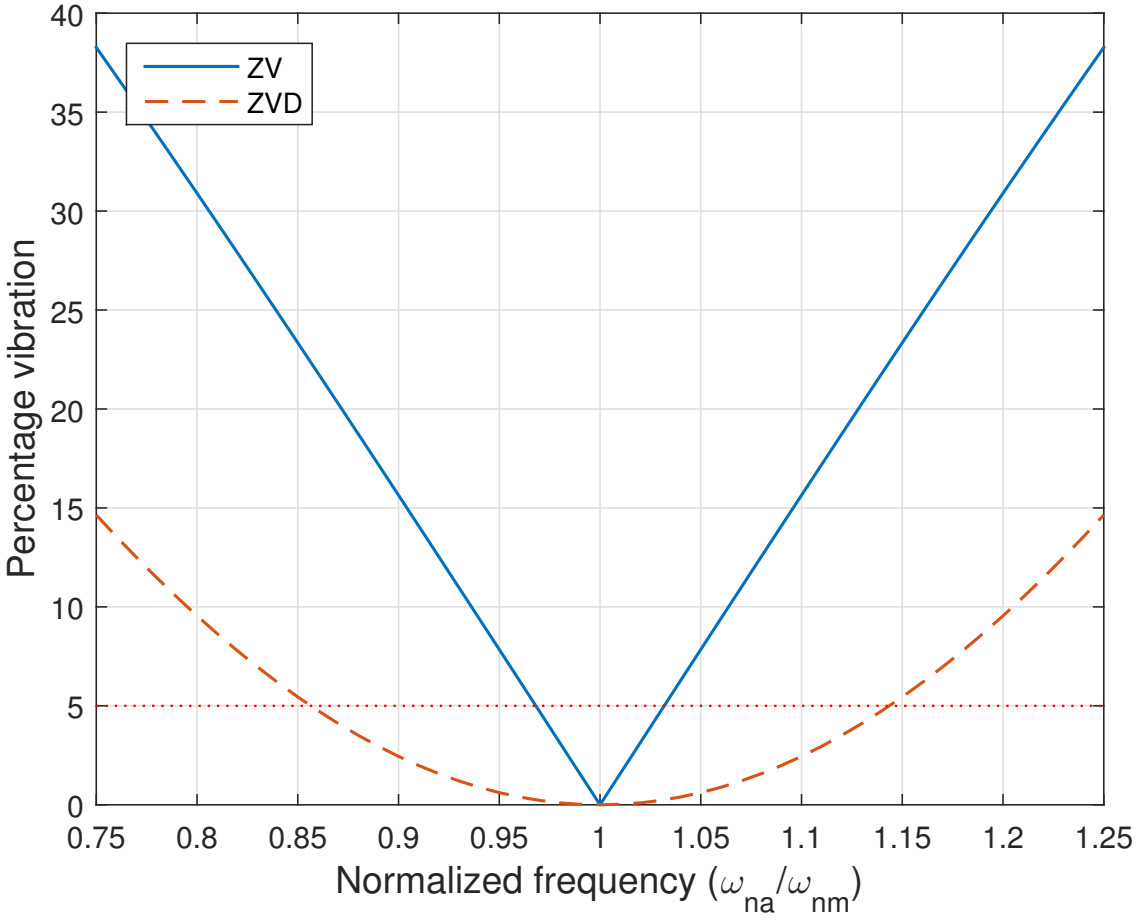

Figure 12: Sensitivity curves for ZV and ZVD shapers. ω_{na} is the actual natural frequency and ω_{nm} is the modeling frequency.

4 Crane Positioning

Command shaping methods described in the chapters 2 and 3 can be utilized for positioning. Command shaping modifies the speed reference in order to remove payload oscillations. This chapter explains positioning with pre-computed commands and input shapers and how they can be integrated into position control. This chapter presents three pre-computation algorithms along with the input shapers.

4.1 Positioning module

A crane positioning module can be implemented in three ways: separate blocks for a positioning and speed reference shaping, a single block which performs both tasks simultaneously or only a positioning block. Blocks can be considered as algorithms. Fig. 13 presents example of swayless positioning when shaping is used. The positioning block calculates a speed reference and the shaping block shapes the reference. A given speed reference is shaped using methods described in the chapters 2 and 3. When the speed reference is reached, both an angle and angular velocity of the payload are zero. The speed reference is zero during the deceleration phase. By varying the speed reference, different positions can reached. In theory, shaping does not affect at the traveled distance if both acceleration and deceleration parts are shaped. However, shaped signals always have longer rise times than the reference signal. The speed profile in the figure can be created using the both pre-computation and input shaping. One of the challenges in implementing the algorithm is that shaping should not cause any positioning error in the traveled distance.

If blocks are separate, they can be easily updated or changed. Fig. 14 shows a block diagram for separate blocks and how it can be integrated with a position control. The position control has a position feedback but it is not mandatory. Possible gear ratios, delays or filters are not included in the figure.

The shaped speed reference is feedforwarded to a speed controller. Precise positioning is hard to achieve without position feedback. Therefore, the position feedback is usually required. The difference between a shaped position reference and the position feedback is proportionally increased and summed to the feedforwarded speed. The output speed v_{out} is fed to a speed controller of a drive. The feedback causes a residual swaying, as it is not shaped. Effect of the feedback can be adjusted by changing the gain of P controller. The results can be improved by moving the shaping block after the position control. However, it increases positioning time significantly and prevents the usage of the pre-computation methods, as they would produce slow results or could be stuck into a recalculation loop. In open-loop control, an actual position is not measured and the shaped speed is just feedforwarded to the speed controller.

4.2 Positioning with Pre-Computed Command

Positioning with pre-computation is the easiest to implement using a single block. Separate blocks for positioning and shaping have multiple problems. When the

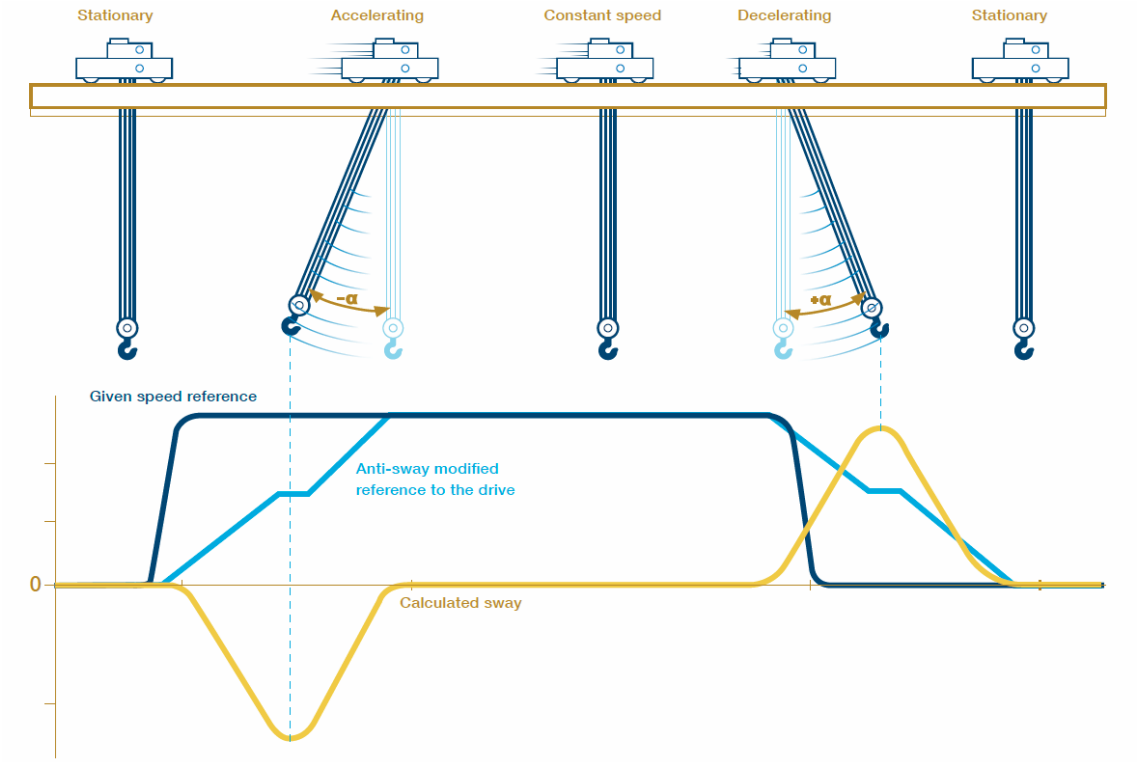

Figure 13: Positioning with command shaping. Calculated sway is angle of the payload, i.e. angle α. [21]

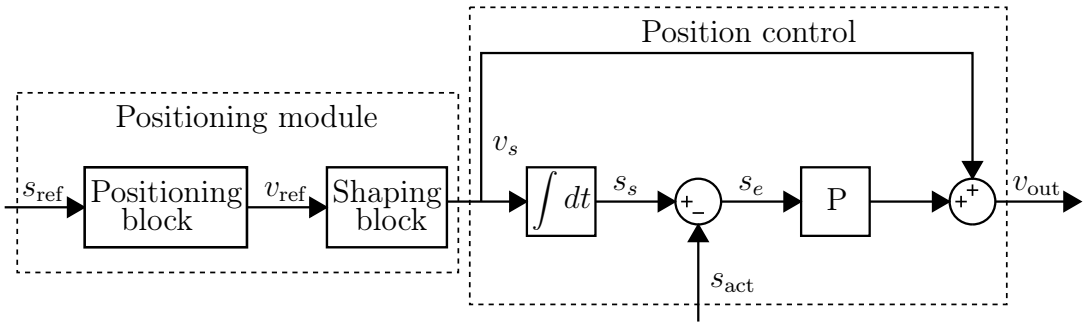

Figure 14: The positioning module and position control. s_{ref} is the position reference, v_{ref} is the speed reference from the positioning block, v_s is the shaped speed reference, s_{act} is the measured actual position, s_s is the shaped position reference, s_e is the position error and v_{out} is the output speed to a speed controller.

shaping block gets a new speed reference, it calculates a new shaped reference. Therefore positioning block needs to calculate a distance traveled with the shaped reference speed in order to give a deceleration command at the right moment. If the position reference is not allowed to change midstream, the implementation of separate blocks is not difficult.

If the position reference is allowed to change during movement, there will be problems. When the position reference changes, a new speed reference is also

calculated. However, if the previous position had not been reached, the trolley has an initial speed and the payload is swaying. This initial swaying is removed with the sway compensation but it causes a positioning error. The positioning block either needs to calculate this positioning error or get it with feedback. Calculation of this positioning error requires information about the sway compensation acceleration and its duration. Calculating sway compensation acceleration in both blocks is completely unnecessary. Using the single block avoids this problem.

In pre-computation, a crane motion profile can be divided into sections. If accelerations are constant, a speed profile is either trapezoidal or triangular. When jerks are given, an acceleration, speed and position can be solved by integrating in parts:

$$j(t) = j_i \tag{65}$$

$$a(t) = a(t_i) + \int_{t_i}^{t} j(x)dx \tag{66}$$

$$v(t) = v(t_i) + \int_{t_i}^{t} a(x)dx \tag{67}$$

$$s(t) = s(t_i) + \int_{t_i}^{t} v(x)dx \tag{68}$$

Subscript i points to the beginning of each section. [24] There are multiple pre-computation approaches. The first approach is to shape acceleration and deceleration phases according to the minimum time strategy. Results are similar to Fig. 13. On the other hand, swayless positioning is possible even without command shaping. In the bang-off-bang control, the deceleration phase is timed appropriately in order to remove swaying of a payload [5]. However, these methods have a few flaws.

The acceleration strategies presented in the section 2.3 only work with a constant acceleration. When accelerations change instantly, jerks are infinite. However, instant acceleration changes are problematic for various reasons: they are difficult to generate accurately using industrial motors and they cause stress on the crane structure. [22] In addition, an exact timing of switches is difficult [23].

Instant accelerations can be avoided by using a sinusoidal speed reference [4]. In this thesis, this method is referred to as trigonometric shaping. Unfortunately, every method has drawbacks. Positioning with the bang-off-bang control and trigonometric shaping only work when an initial speed of the trolley is zero and the pendulum has no swaying.

Pre-computation methods have to include the sway compensation, which was presented in the section 2.4, in order to remove an initial swaying. Whenever the position reference changes, there will be an initial swaying. If a pendulum has sway, it is compensated before positioning. Due to the linearization of the crane, accelerations could be summed together and hence decrease positioning time. However, the summation of accelerations complicates implementation, as there would be multiple scenarios depending on the durations of accelerations. Nevertheless, when the summation of accelerations is not used, positioning time is only increased in cases where the sway compensation is used.

4.2.1 Minimum Time Strategy

In the minimum time strategy, acceleration changes are instantaneous. Nevertheless, motion of a crane can be divided into parts. Swayless positioning is obtained when both acceleration and deceleration phases are shaped according to the minimum time strategy. The shaped speed reference depends on two variables: the input ramp time t_{acc} and the travel speed v_t. If a duration of the input ramp is t_{acc}, then the shaped speed has rise time of $t_{\text{acc}} + \tau/2$. When $t_{\text{acc}} < \tau/2$, shaped reference looks like in Fig. 15. A reference speed to which a trolley is accelerated to is referred to as a travel speed. During constant speed phase, the trolley moves at the travel speed.

A motion profile can be divided into seven sections and each section solved

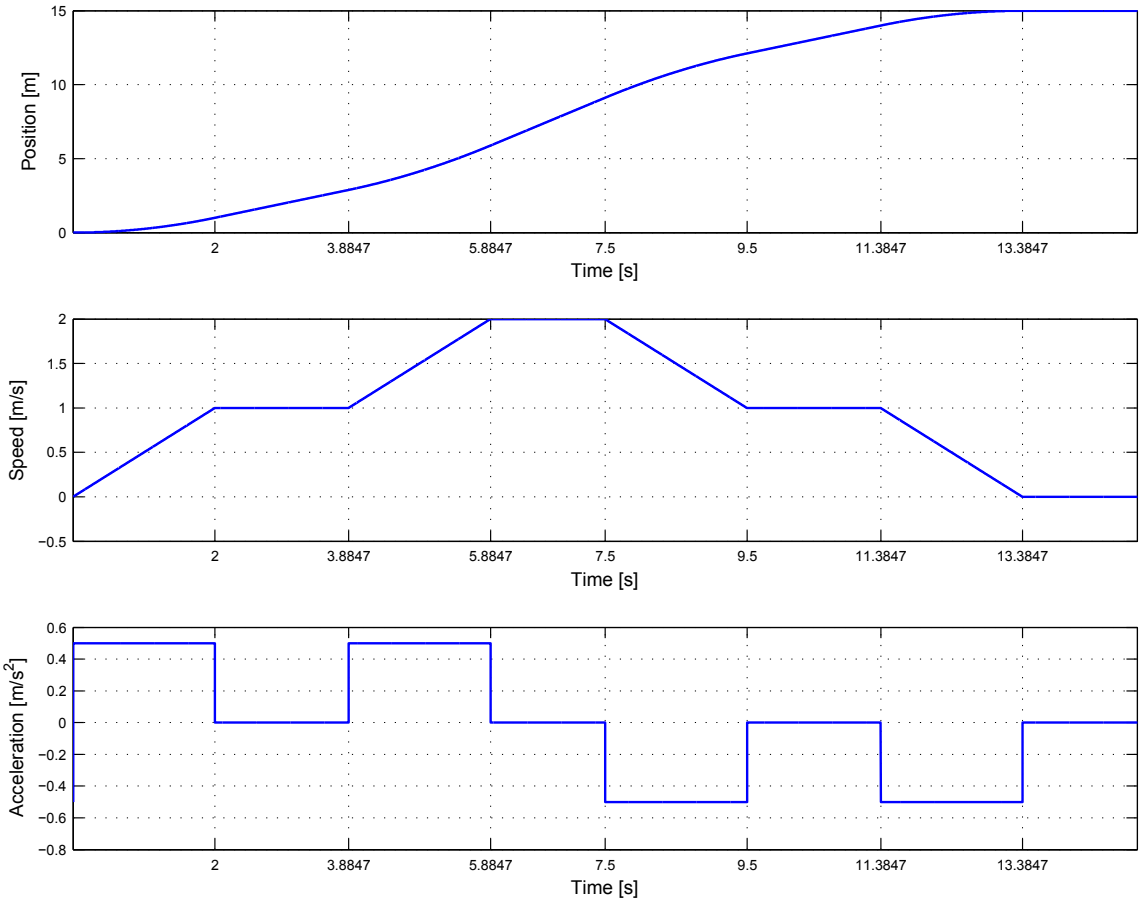

Figure 15: The motion profile, when $t_{acc} < \tau/2$. Parameters are $s_{\text{ref}} = 15$ m, $\tau = 7.7695$ s, $t_{\text{acc}} = 2$ s and travel speed $v_t = 2$ m/s.

separately. The acceleration is

$$a(t) = \begin{cases} a_{\text{acc}} & t < t_1 \\ 0 & t_1 \leq t < t_2 \\ a_{\text{acc}} & t_2 \leq t < t_3 \\ 0 & t_3 \leq t < t_4 \\ -a_{\text{dec}} & t_4 \leq t < t_5 \\ 0 & t_5 \leq t < t_6 \\ -a_{\text{dec}} & t_6 \leq t < t_7 \end{cases} \tag{69}$$

where a_{acc} is the positioning acceleration and a_{dec} is the positioning deceleration. Integrating Eq. (69) produces a speed:

$$v(t) = \begin{cases} v_0 + a_{\text{acc}} t & t < t_1 \\ v_1 & t_1 \leq t < t_2 \\ v_2 + a_{\text{acc}} t & t_2 \leq t < t_3 \\ v_3 & t_3 \leq t < t_4 \\ v_4 - a_{\text{dec}} t & t_4 \leq t < t_5 \\ v_5 & t_5 \leq t < t_6 \\ v_6 - a_{\text{dec}} t & t_6 \leq t < t_7 \end{cases} \tag{70}$$

where v_0 is the initial speed, i.e. the speed when positioning starts. $v_0 = v_{\text{act}}$ if there is no sway compensation. A position is

$$s(t) = \begin{cases} s_0 + v_0 t + \frac{1}{2} a_{\text{acc}} t^2 & t < t_1 \\ s_1 + v_1 t & t_1 \leq t < t_2 \\ s_2 + v_2 t + \frac{1}{2} a_{\text{acc}} t^2 & t_2 \leq t < t_3 \\ s_3 + v_3 t & t_3 \leq t < t_4 \\ s_4 + v_4 t - \frac{1}{2} a_{\text{dec}} t^2 & t_4 \leq t < t_5 \\ s_5 + v_5 t & t_5 \leq t < t_6 \\ s_6 + v_6 t - \frac{1}{2} a_{\text{dec}} t^2 & t_6 \leq t < t_7 \end{cases} \tag{71}$$

In Eq. (71) initial position $s_0 = 0$ as we need to calculate only acceleration and deceleration distances. The initial position is taken into account in the target position s_t. However, the sway compensation changes the target position. The target position for the minimum time strategy is

$$s_t = s_{\text{ref}} - s_{\text{act}} - v_{\text{act}}(t_d + t_w) - \frac{1}{2} a_c t_d^2 \tag{72}$$

where s_{ref} is the reference position, v_{act} is the actual speed, t_d is the duration and t_w is the waiting time of the sway compensation acceleration a_c, and s_{act} is the actual position. The acceleration distance can be solved from Eqs. (70) and (71):

$$s_{\text{acc}} = v_0 \left(\frac{\tau}{2} + t_{\text{acc}} \right) + a_{\text{acc}} \left(\frac{t_{\text{acc}} \tau}{2} + t_{\text{acc}}^2 \right) \tag{73}$$

The deceleration distance can be solved similarly and it is

$$s_{\mathrm{dec}} = a_{\mathrm{dec}} \left(\frac{t_{\mathrm{acc}} \tau}{2} + t_{\mathrm{acc}}^2 \right) \tag{74}$$

Duration of the constant speed phase is

$$t_{\mathrm{c}} = \frac{s_t - s_{\mathrm{acc}} - s_{\mathrm{dec}}}{v_{\mathrm{t}}} \tag{75}$$

When $t_c < 0$, the constant speed phase is omitted and accelerations must be reduced. If the accelerations are not reduced, positioning goes over the target. With new acceleration values, the trolley starts to decelerate right after the acceleration ends. New values for the positioning acceleration and deceleration are

$$a_{\mathrm{acc}} = \frac{s - \frac{3}{4} v_0 (2t_{\mathrm{acc}} + \tau)}{t_{\mathrm{acc}} \tau + 2t_{\mathrm{acc}}^2} \tag{76}$$

$$a_{\mathrm{dec}} = \frac{v_0}{2t_{\mathrm{acc}}} + a_{\mathrm{acc}} \tag{77}$$

Fig. 16 shows the speed and the acceleration profiles, when $t_{\mathrm{acc}} > \tau/2$. The acceleration, speed and position are solved similarly as in case $t_{\mathrm{acc}} < \tau/2$. Even though graphs in Figs. 15 and 16 are different, their results are the same. Eqs. (73) - (77) also apply for the case $t_{\mathrm{acc}} > \tau/2$.

4.2.2 Bang-Off-Bang Control

Shaping of acceleration and deceleration phases is not mandatory. Without command shaping, positioning is possible by timing the deceleration phase appropriately. This method is referred to as bang-off-bang control. Bangs refer to moments when accelerations are turned on, e.g., bang-off-bang means that first acceleration is turned on, then off and finally on. Fig. 17a shows a pendulum movement in the phase plane during bang-off-bang control. The acceleration and deceleration must have identical duration and magnitude or there will be residual swaying. The deceleration phase begins at the time $\tau + z\tau$ where z is a number of full constant speed cycles in the phase plane. [5] Higher the number z, longer the travel time. The speed profile and sway are shown in Fig. 17b.

The durations of the acceleration and deceleration phases are t_{acc} and the duration of the constant speed phase is $(z+1)\tau - t_{\mathrm{acc}}$. The total travel distance (i.e. target position) is

$$s_t = (z+1)\tau t_{\mathrm{acc}} a_{\mathrm{acc}} \tag{78}$$

where a_{acc} is the positioning acceleration. The target position for the bang-off-bang control is

$$s_t = s_{\mathrm{ref}} - s_{\mathrm{act}} - v_{\mathrm{act}}(t_d + t_w) - \frac{1}{2} a_c t_d^2 - (v_{\mathrm{act}} + a_c t_d + a_{\mathrm{sp}} t_{\mathrm{sp}})(t_{\mathrm{sp}} + \frac{\tau}{2}) \tag{79}$$

where s_{ref} is the reference position, v_{act} is the actual speed, t_d is the duration and t_w is the waiting time of the sway compensation acceleration a_c, s_{act} is the actual

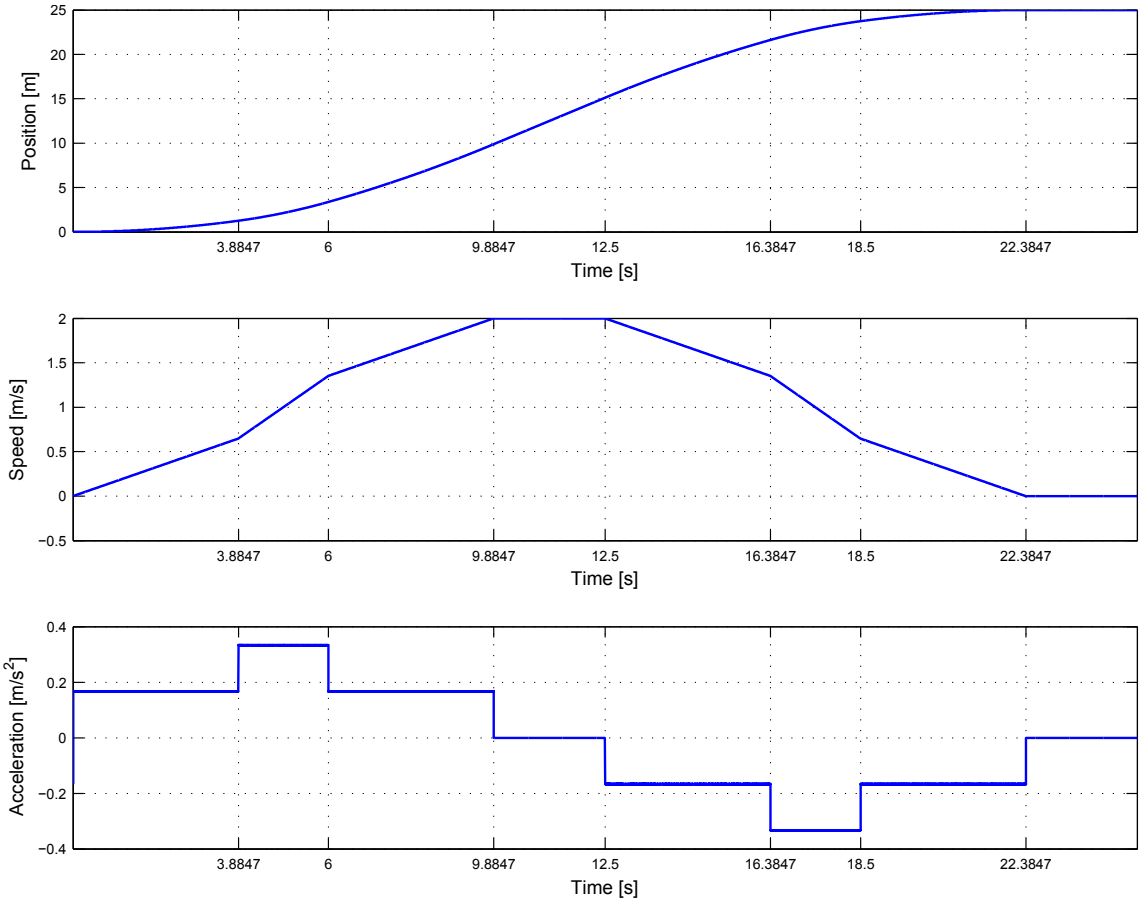

Figure 16: The motion profile, when $t_{acc} > \tau/2$. Parameters are $s_{\text{ref}} = 25$ m, $\tau = 7.7695$ s, $t_{\text{acc}} = 6$ s and $v_t = 2$ m/s

position, a_{sp} is the speed providing acceleration, t_{sp} is duration of the acceleration pulse in the speed providing acceleration and τ is the period of the pendulum. The speed providing acceleration uses the minimum time strategy. The acceleration solved from Eq. (78) is

$$a_{\text{acc}} = \frac{s_t}{(z+1)\tau t_{\text{acc}}} \tag{80}$$

The number z is zero at first. If $a_{\text{acc}} > a_{\text{max}}$, z is increased by one until the maximum acceleration is not exceeded. The pendulum sways the whole duration of the movement which can pose a safety hazard.

Positioning with bang-off-bang control only works when an initial speed is zero and the pendulum does not sway. An initial swaying is removed with the sway compensation and after that the speed providing acceleration drives speed of the trolley to zero. If the trolley has the initial speed but the payload is not swaying, only the speed providing acceleration is used. In total, bang-off-bang control uses three accelerations.

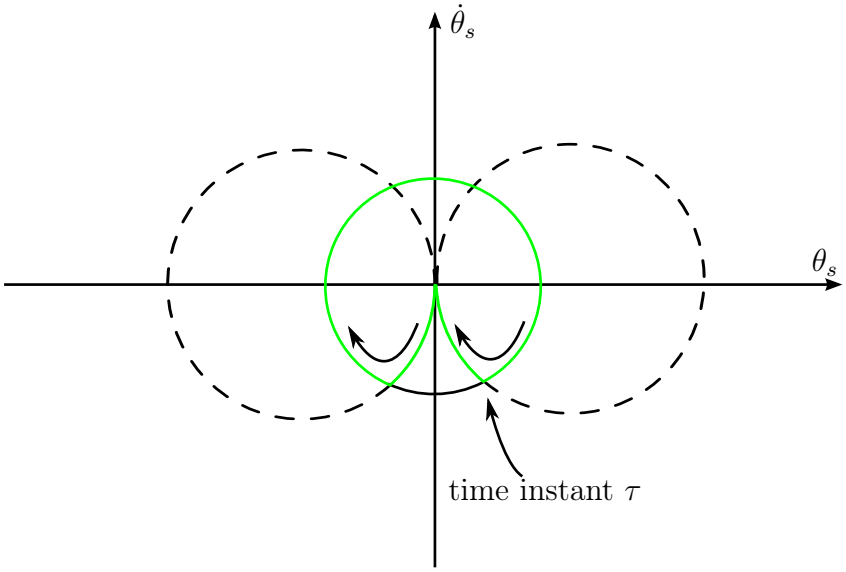

(a) Phase plane

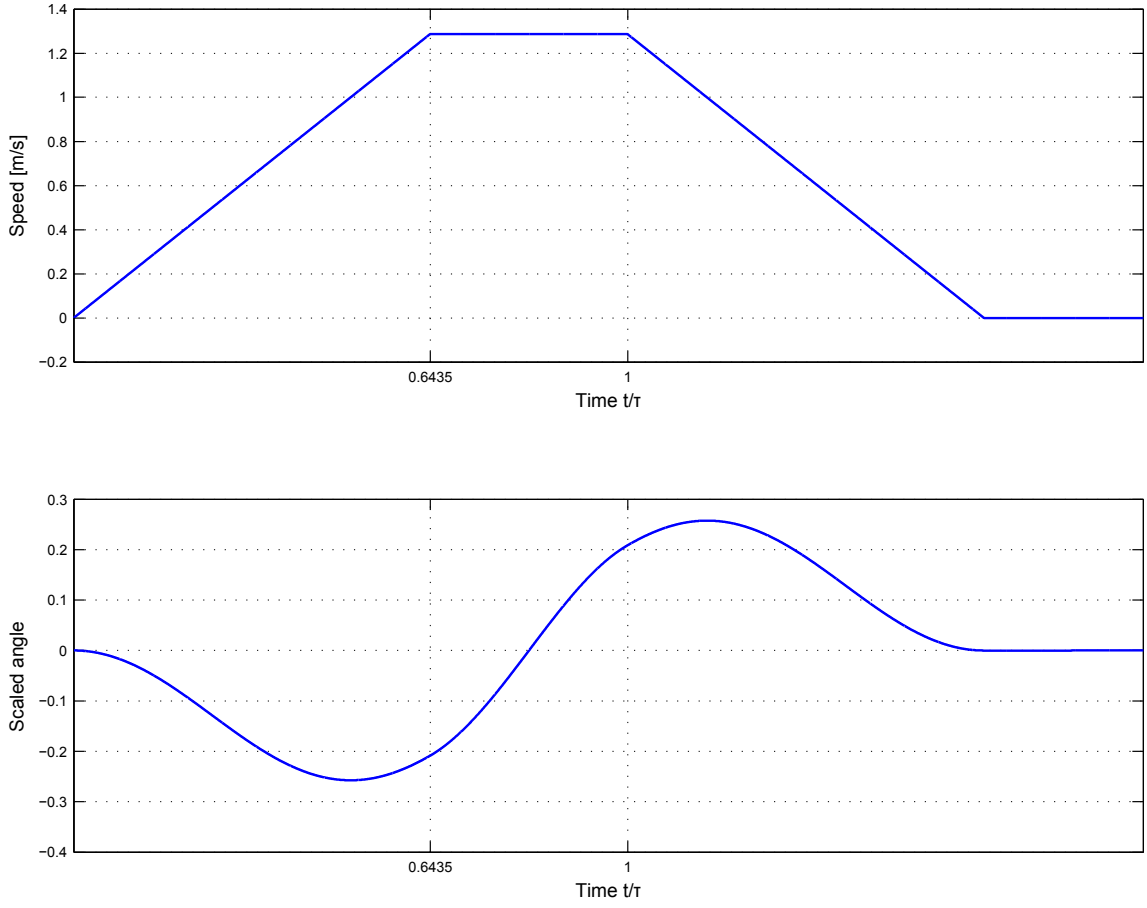

(b) Time domain

Figure 17: Positioning with bang-off-bang control. (a) The movement in the phase plane. Path of the pendulum is shown with the green line. (b) The movement in time domain. In this example parameters are $t_{\text{acc}} = 5$ s, $\tau = 7.7695$ s and $a_{\max} = 1$ m/s^2.

4.2.3 Trigonometric Shaping

The third pre-computed positioning approach uses a sinusoidal speed reference. This approach is referred to as trigonometric shaping, in which a position reference is shaped by using cosine function. If the target position is given as a step reference s_t, the shaped position reference is

$$s_s = \begin{cases} \frac{1}{2} s_t \left[1 - \cos(\frac{\omega_n t}{\alpha})\right] & 0 \leq t \leq (\alpha\pi/\omega_n) \\ s_t & t > (\alpha\pi/\omega_n) \end{cases} \tag{81}$$

where α is the travel time factor and ω_n is the natural frequency of the pendulum. Acceptable values of α are $3, 5, 7, \ldots (2n+1)$ where n is an integer. [4] Initially $\alpha = 3$ but it is increases by increments of 2 as long as the maximum acceleration or the maximum speed are exceeded. The fastest motion is achieved with $\alpha = 3$ but it also causes a largest sway. The acceleration is lowered by increasing α. Target position of the trigonometric shaping is calculated with Eq. 79. The speed reference is

$$v_s = \begin{cases} \frac{\omega_n s_t}{2\alpha} \sin(\frac{\omega_n t}{\alpha}) & 0 \leq t \leq (\alpha\pi/\omega_n) \\ 0 & t > (\alpha\pi/\omega_n) \end{cases} \tag{82}$$

Trigonometric shaping has the same drawbacks as the bang-off-bang control. Positioning only works when the pendulum is at rest in the beginning and speed of a trolley is zero. Therefore, the sway compensation removes an initial swaying and the speed providing acceleration drives the speed of the trolley to zero.

4.3 Positioning with Input Shaping

An input shaper delays parts of a speed reference, and thus removing oscillations of a payload. Positioning with input shaping can be implemented multiple ways as input shaper keeps time integral of input and output the same. Therefore, implementing a positioning module is easy when using two blocks. A positioning block takes care that correct position is reached. A positioning algorithm can be implemented any way possible. A speed reference from the positioning block is shaped using input shaping. The input shaper does not require sway compensation like pre-computation schemes. Therefore, changing a position reference does not require any extra procedures.

In addition, input shaping can also shape a position reference instead of a speed reference. No matter what kind of signal is used, input shaper works the same way in all cases. Block diagram for shaping of a position reference is illustrated in Fig. 18. IPO stands for an interpolator which shapes a step reference into a smoother signal. Output of the interpolator depends on the maximum speed and acceleration limits. The position reference from the interpolator is given to the input shaper. The shaped position reference is fed to the position control. Feedforward loop has a low-pass filter since the position control has a derivation which is sensitive to a noise and disturbances.

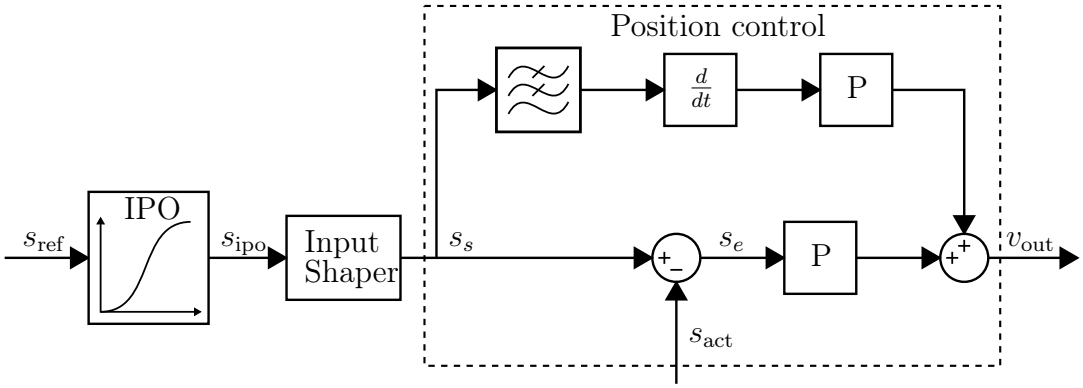

Figure 18: Shaping of the position reference. IPO stands for an interpolator. s_{ref} is the step position reference, s_{ipo} is the position reference from the interpolator, s_s is the shaped position reference, s_e is the position error, s_{act} is the measured actual position and v_{out} is the output speed to the speed controller.

5 Simulations

The positioning algorithms described in the chapter 4 were tested using Simulink simulations. The aim of the simulations was to test performance of the algorithms for point-to-point positioning. This chapter presents the implementation of the simulation model and the simulation results.

5.1 Implementation of the Simulation Model

A block diagram of the simulation model is shown in Fig 19. Position and speed feedbacks are not used and for a simplification, a drive and motor are not modeled. A positioning module is implemented according to the corresponding algorithm, e.g., the minimum time strategy uses a single block, in which both positioning and shaping are performed. The crane model is based on Eq. (8). An angle is obtained by integrating an angular acceleration which is solved from Eq. (8):

$$\ddot{\theta} = -\frac{g}{L}\sin(\theta) - \frac{2\dot{L}\dot{\theta}}{L} - \frac{\ddot{x}}{L}\cos(\theta) - 2\xi\sqrt{\frac{g}{L}}\dot{\theta} \tag{83}$$

The crane Simulink model is shown in Fig. 20. Inputs of the crane model are the shaped acceleration a_s, the length of the rope L_a and the damping ratio ξ_a. The shaped speed reference is derived ($a_s = \ddot{x}$) and feedforwarded to the crane model, hence simplifying observation of functionality of the algorithms.

Input parameters of the simulation model are the position reference s_{ref}, the length of the rope L, the travel speed v_t, the ramp time t_{acc} and the damping ratio ξ. A subindex m refers to model and subindex a for actual. In addition, the input shapers have one additional parameter: the size of a ring buffer N_b. Output variables are the traveled distance s_s, the shaped speed v_s and the angle of the pendulum θ. The maximum acceleration is defined as $a_{\max} = v_t/t_{\text{acc}}$.

5.1.1 Positioning module

Pre-computation algorithms were implemented with a single block. As discussed in the chapter 4, the sway compensation is incorporated into pre-computation

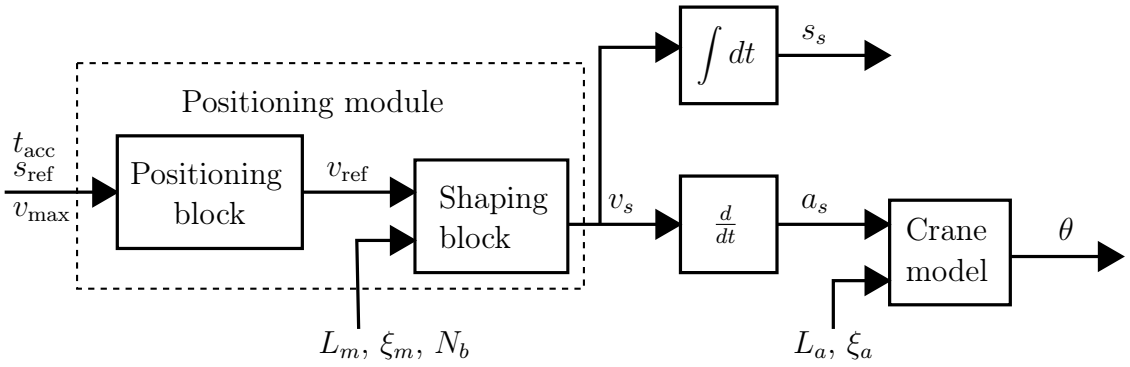

Figure 19: Block diagram of the simulation model.

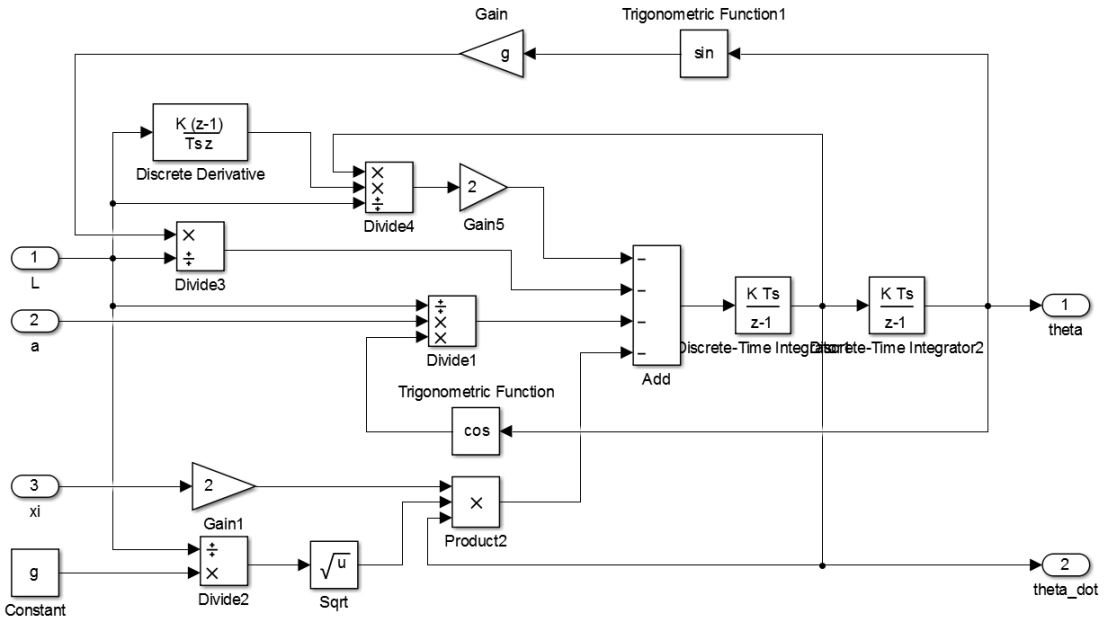

Figure 20: Crane Simulink model.

algorithms. Without the sway compensation, the algorithms would work only in limited situations. With this addition, the algorithms have multiple phases that are executed in succession. The minimum time strategy has two phases: sway compensation and positioning. An initial sway is compensated first and after that a trolley is positioned. The bang-off-bang control and trigonometric shaping have three phases: sway compensation, speed removal and positioning. When using the bang-off-bang control or trigonometric shaping, positioning can only begin when the trolley and payload are at rest. In the algorithms, the sway tracking was implemented by numerically integrating Eq. (83).

Unlike pre-computation algorithms, the positioning module for the input shapers used separate blocks. A positioning block creates trapezoidal speed curve, thus enabling comparison of the input shapers and pre-computation algorithms. This positioning algorithm is demonstrated in Fig. 21. A constant speed phase exists during normal operation, which is presented in Fig. 21a. The duration of the acceleration and deceleration phases are t_{acc} and the duration of the constant speed phase is calculated from Eq. (75). The deceleration phase does not need to start at time τ as in the bang-off-bang control. The accelerations are

$$a_{\mathrm{acc}} = \frac{v_t - v_{\mathrm{act}}}{t_{\mathrm{acc}}} \tag{84}$$

$$a_{\mathrm{dec}} = \frac{v_t}{t_{\mathrm{acc}}} \tag{85}$$

where v_t is the travel speed and v_{act} is the actual speed. If the duration of the constant speed phase is less than zero, the constant speed phase is omitted. As a result, the speed profile is triangular and new accelerations are calculated. This

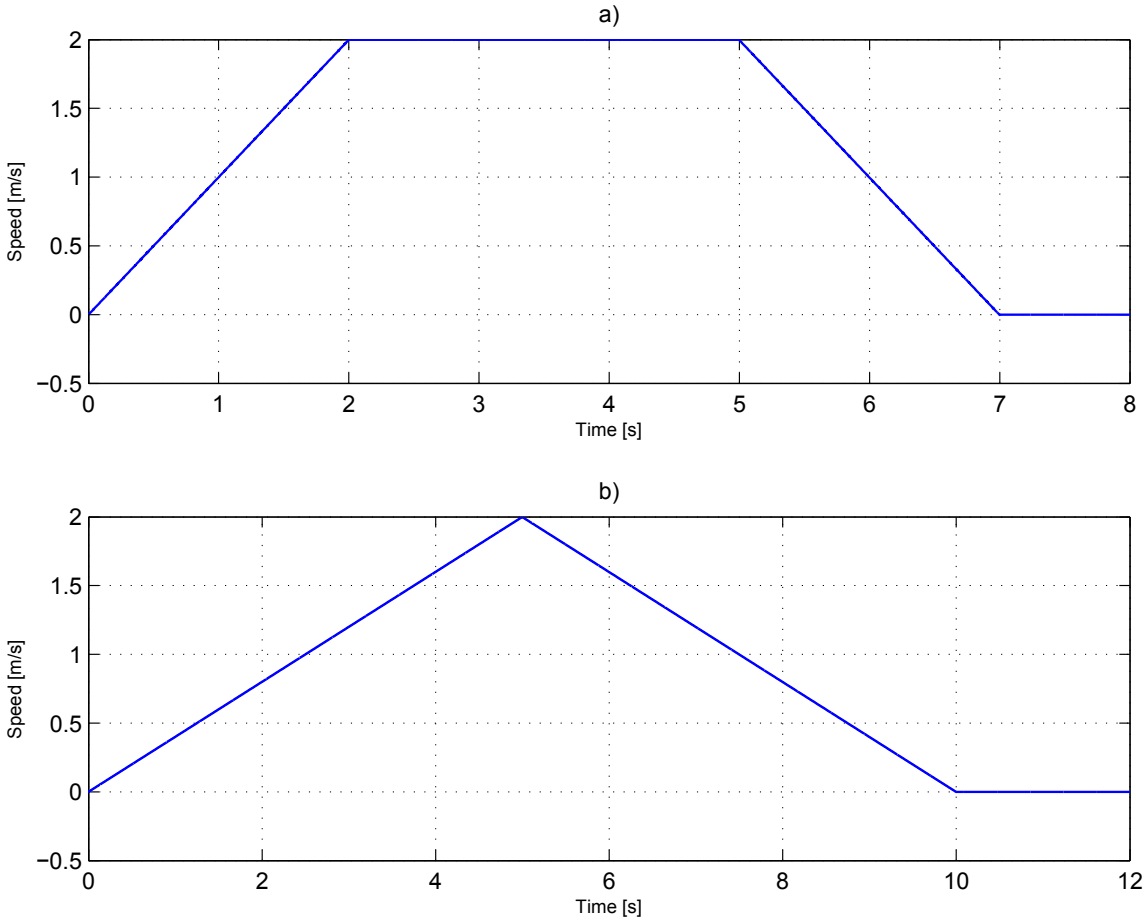

Figure 21: Positioning algorithm used with input shaping. Parameters are $s_{\text{ref}} = 10$ m and $v_t = 2$ m/s. a) Constant speed phase is reached when $t_{\text{acc}} = 2$ s. b) Constant speed phase is omitted when $t_{\text{acc}} = 5$ s.

is displayed in Fig. 21b, in which positioning contains only the acceleration and deceleration phases. New values for the accelerations are

$$a_{\text{acc}} = \frac{s_t - 2t_{\text{acc}}v_{\text{act}}}{2t_{\text{acc}}^2} \tag{86}$$

$$a_{\text{dec}} = \frac{v_0}{t_{\text{acc}}} + a_{\text{acc}} \tag{87}$$

where s_t is the target position.

The shaping block used input shaping, in which the output signal consists partially of input and delayed signals. In the shaper, an input signal is sampled and samples are added to a ring buffer which acts as a delay. A ZV shaper has one buffer and a ZVD shaper has two. Size of the ring buffer describes how many samples a delayed signal contains. Fig. 22 shows a ring buffer with the size of 16. Depending on the buffer size and delay, the sampling time of the buffer is either $T_d/(2N_b)$ or T_d/N_b. If the sampling time is $T_d/(2N_b)$, a written value is read after time $T_d/2$. Upon each sampling, a new value is stored to an element indicated by a pointer. After writing a

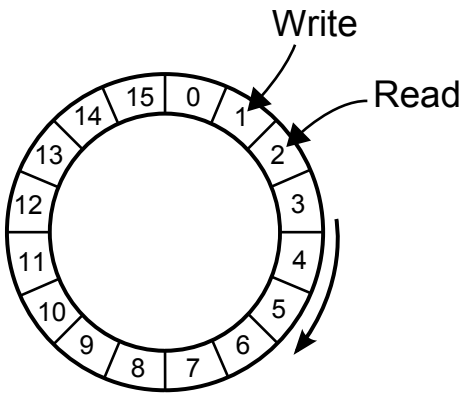

Figure 22: A ring buffer with size of 16. Values are stored in clockwise direction.

sample, the index of the pointer is increased by one so that it points to an element, in which the oldest value is stored. This element is read and after that new sampling phase begins. Results can be improved by increasing the buffer size. However, if the sampling is smaller than task execution cycle, shaper works incorrectly as the delayed signals occur too late. Unfortunately, buffers require memory which is one of the drawbacks of input shaping.

5.2 Simulation Results

The algorithms were compared in different situations in order to determine the most effective algorithm. Compared characteristics of the algorithms included positioning accuracy, positioning time and robustness. The sample time of the simulations was 1 ms. Size of the buffer can be chosen freely but too small buffer is inaccurate and too large causes incorrect delays. For all tests, buffer size was kept as 200.

5.2.1 Point-to-Point Positioning

Correct system parameters

The simplest case is point-to-point positioning with a constant rope length and correct system parameters (ω and ξ). Additionally, the position reference does not change during simulation. Fig. 23 shows positioning with different algorithms when position reference is given as a step input. Parameters are $t_{\text{acc}} = 3$ s, $v_t = 2$ m/s, $L_a = 16$ m, $s_{\text{ref}} = 15$ m, $\xi_a = 0$ and $N_b = 200$. $L_m = L_a$, as the system parameters are correct.

All methods reach the end point without residual swaying. The minimum time strategy and the ZV shaper produce identical results and they do not cause large sway during movement when compared to other methods. The ZVD shaper causes the least sway during movement but it is the slowest method. Bang-off-bang and trigonometric shaping have one major disadvantage: the pendulum sways greatly during the movement. This can pose a safety risk if a load is heavy and an angle of the sway is large. Additionally, swaying causes stress to crane structure. Nevertheless, bang-off-bang control and trigonometric shaping are fast because of $z = 0$ and $\alpha = 3$.

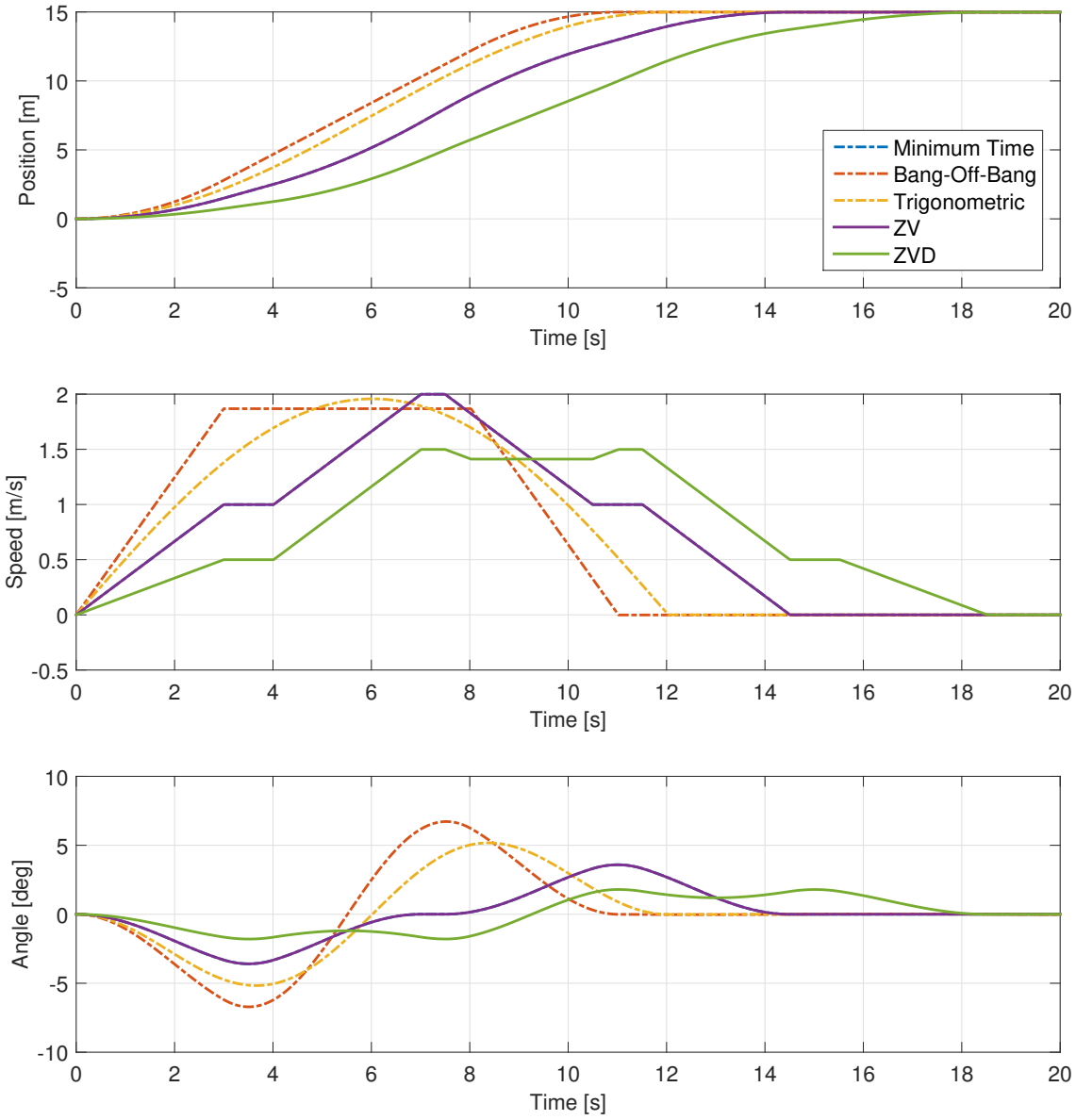

Figure 23: Point-to-point positioning when parameters are $s_{\text{ref}} = 15$ m, $t_{\text{acc}} = 3$ s, $v_t = 2$ m/s, $L_a = 16$ m and $\xi_a = 0$.

Fig. 24 shows another point-to-point positioning test, in which conditions are the same as in the previous test. In this second test, parameters are $s_{\text{ref}} = 4$ m, $t_{\text{acc}} = 4$ s, $v_t = 4$ m/s, $L_a = 6$ m and $\xi_a = 0$. Now the minimum time strategy and the ZV shaper do not produce identical results. This is due to that acceleration and deceleration phases do not happen simultaneously in the minimum time strategy. In the ZV shaper, the deceleration phase begins before the acceleration phase has ended, which leads to a constant speed. Duration difference between minimum time strategy and ZV shaping is $\tau/2$. Also in this test, the bang-off-bang control and trigonometric shaping produce fast results. However, the trigonometric shaping sways significantly more than other methods during movement. Overall, it can be summarized that

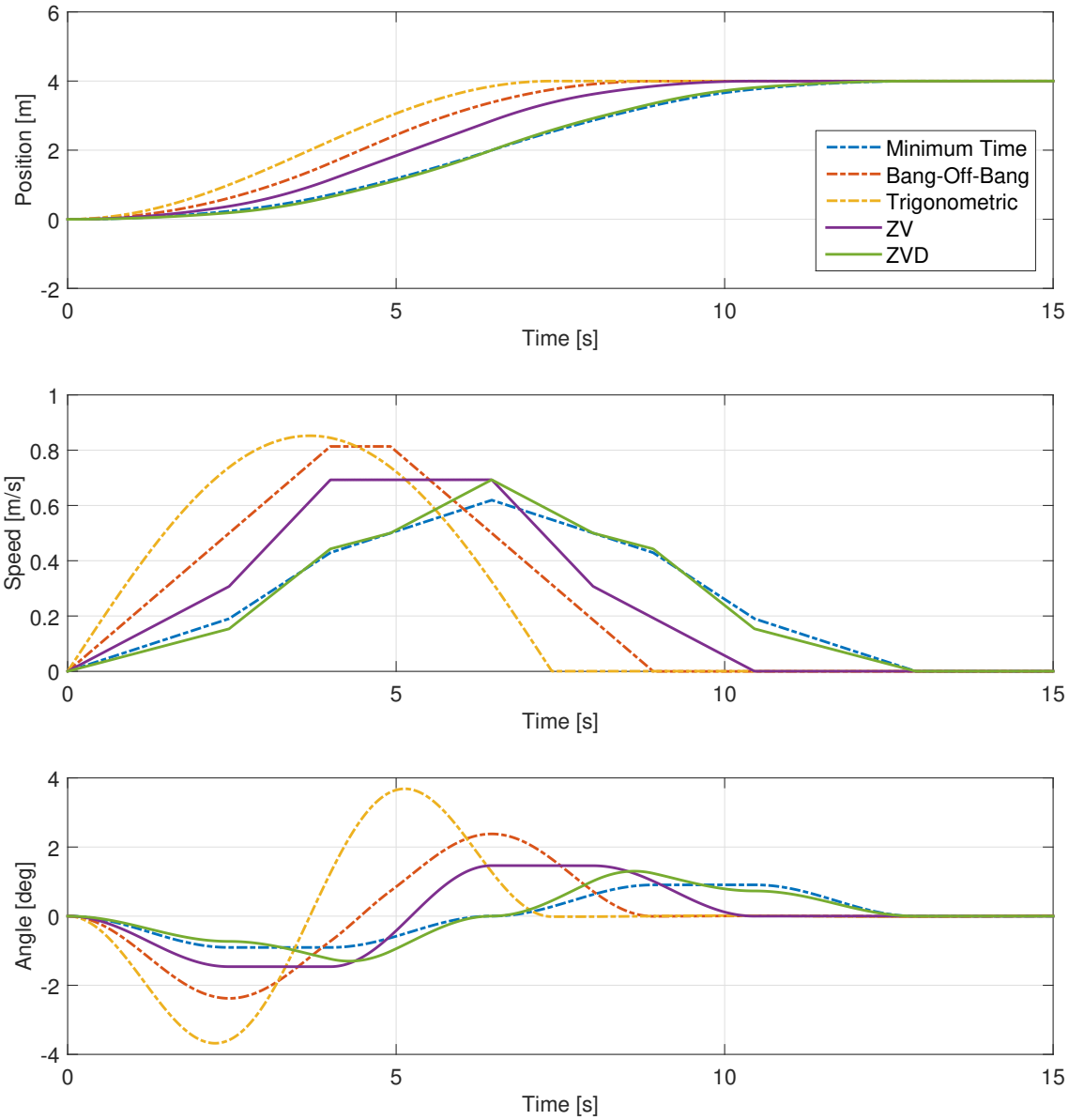

Figure 24: Point-to-point positioning when parameters are $s_{\text{ref}} = 4$ m, $t_{\text{acc}} = 4$ s, $v_t = 4$ m/s, $L_a = 6$ m and $\xi_a = 0$.

faster the positioning, larger the sway during the movement.

The effects of damping are demonstrated in Fig. 25. System parameters are correct and parameters values are $s_{\text{ref}} = 11$ m, $t_{\text{acc}} = 6$ s, $v_t = 2$ m/s, $L = 24$ m and $\xi_a = 0.1$. The ZV and ZVD shapers work without problems when the system has damping. In contrast, pre-computation approaches leave some residual swaying, as they take damping into account only in the sway tracking. Nevertheless, residual swaying caused by the light damping is quite small. A larger damping ratio would cause larger error but the error would damp faster. However, damping does not cause severe problems if accelerations are kept small.

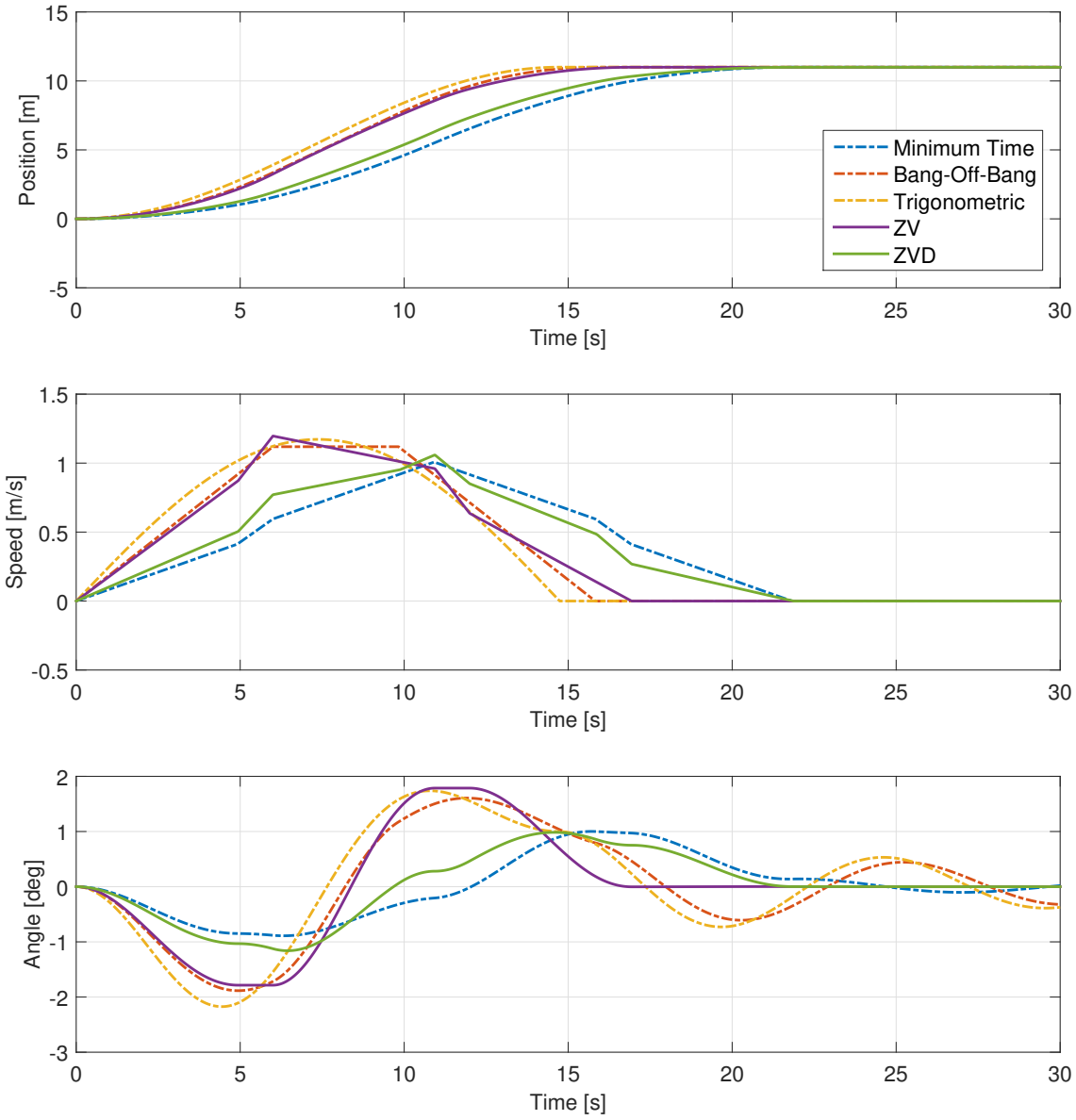

Figure 25: Point-to-point positioning of a damping crane. Parameters are $s_{\text{ref}} = 11$ m, $t_{\text{acc}} = 6$ s, $v_t = 2$ m/s, $L_a = 24$ m and $\xi_a = 0.1$.

Incorrect system parameters

Unlike in the previous tests, real crane systems always have some inaccuracy in measurements of the length of the rope and damping ratio. Sometimes length is calculated instead of direct measurement, e.g. it can be calculated from a motor encoder feedback signal. In order to diminish the measurement errors of the system parameters, algorithm needs to be robust. Fig. 26a shows positioning when the model has incorrect frequency ω_n, i.e. the length of the rope is incorrect. Parameters are the same as in Fig. 24, i.e. $s_{\text{ref}} = 4$ m, $t_{\text{acc}} = 4$ s, $v_t = 4$ m/s, $L_a = 6$ m and $\xi_a = \xi_m = 0$.

With the tested parameter values, residual swaying increases greatly when the

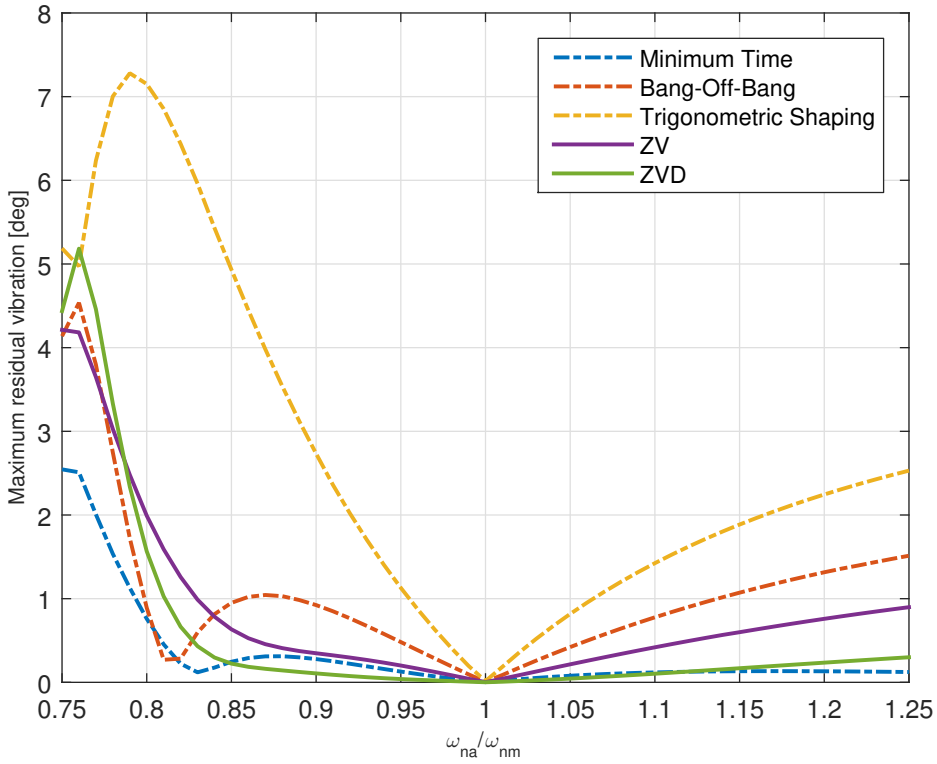

(a) Incorrect frequency.

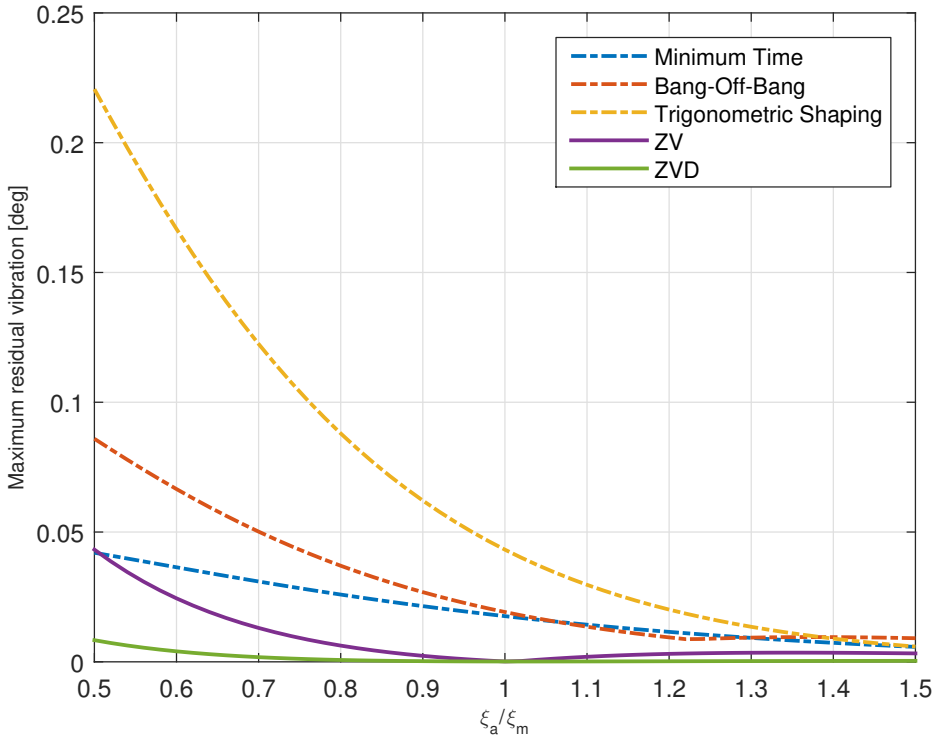

(b) Incorrect damping ratio.

Figure 26: Residual swaying when system parameters are incorrect. Other parameters are $s_{\text{ref}} = 4$ m, $t_{\text{acc}} = 4$ s, $v_t = 4$ m/s and $L_a = 6$ m.

modeling frequency is larger than the actual frequency. In addition, an increment of the swaying is not linear. When the modeling frequency is smaller than the actual frequency, the residual swaying increases only slightly. The trigonometric shaping is the most sensitive to the frequency error and hence making it unfavorable choice. In this test, the minimum time method outperforms the other methods. Although the ZVD shaper performs only slightly worse than the minimum time strategy.

Fig. 26b shows residual swaying when the damping ratio is incorrect. Parameters are the same as in the previous test except that $\xi_m = 0.2$. The maximum residual vibration is calculated from 20 seconds onwards. The shapers do not leave residual vibration when $\xi_a/\xi_m = 1$ but pre-computation methods leave some. However, the residual swaying is very small. When the actual damping ratio is smaller than the model damping ratio, residual vibration increases slightly. When the ratios are the other way round, a residual swaying of the pre-computation methods decreases. On the other hand, residual vibration of the input shapers increases only slightly. Overall, an incorrect damping ratio is not a particularly noteworthy error source.

5.2.2 Changing Position Reference

Sometimes a crane operator may want to change a position reference before an initial reference has been reached. Fig. 27 shows a case where position reference is changed. The initial position reference is $s_{\text{ref}} = -5$ m and the final reference is $s_{\text{ref}} = 20$ m. A moment when the reference changes is at time $t = 3$ s. System parameters are correct and parameter values are $t_{\text{acc}} = 2$ s, $v_t = 4$ m/s, $L_a = 5$ m and $\xi_a = 0$.

When a position reference changes, payload has more or less swaying. The pre-computation algorithms compensate an initial swaying before positioning. After the sway compensation, trigonometric shaping and bang-off-bang can begin positioning only when a trolley is at rest and hence they require deceleration to zero speed. In contrast, the minimum time strategy starts positioning right after the sway compensation. This advantage makes the minimum time strategy the fastest pre-computation method in case of reference change.

Shapers do not have similar limitations and they do not require sway compensation. Due to the delaying nature of the shapers, they can immediately start to follow the new reference as the initial sway is compensated with delayed signals. Because pre-computation methods are implemented to perform each phase in succession, they are usually slower than input shapers. In this example, pre-computation algorithms are a few seconds slower than the ZV shaper.

5.2.3 Variable Rope Length

Hoisting movement is often needed during positioning for maximizing the productivity. However, hoisting causes more difficulties. Hoisting changes the natural frequency ω_n and hence creating a problem for input shapers as they are implemented for constant frequency. Pre-computation algorithms also work only at constant frequency. Nevertheless, a motion profile can be recalculated every time the frequency changes. Recalculations happen at each cycle as long as hoisting occurs. After hoisting,

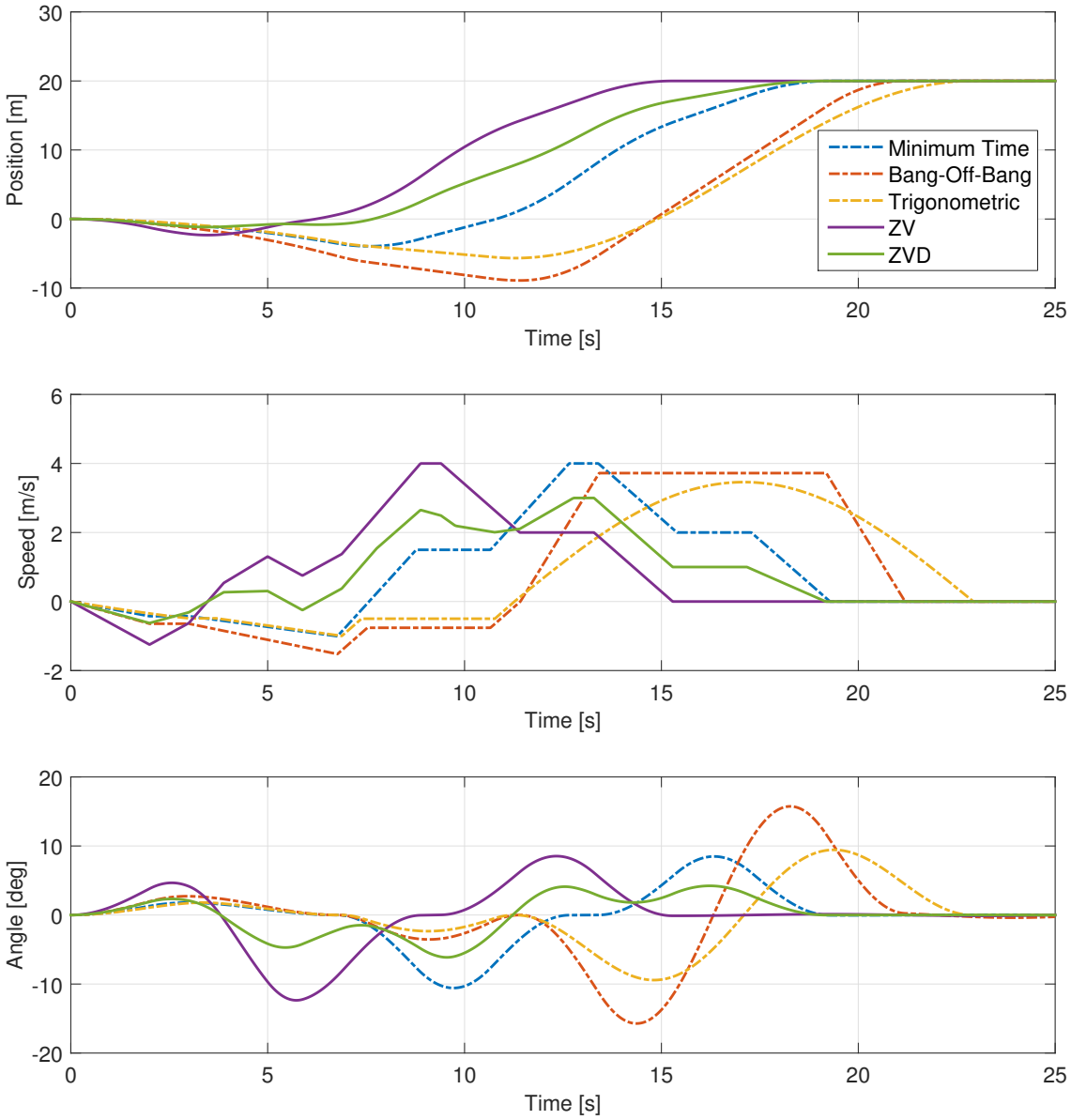

Figure 27: Positioning with changing position reference. Position reference changes at time $t = 3$ s. The initial reference is $s_{\text{ref}} = -5$ m and the final reference is $s_{\text{ref}} = 20$ m. Other parameters are $t_{\text{acc}} = 2$ s, $v_t = 4$ m/s, $L_a = 5$ m and $\xi_a = 0$.

pre-computation algorithms start to work normally. If hoisting takes long, pre-computation schemes produce slow results.

Positioning during hoisting is demonstrated in Fig. 28. The initial rope length is 5 m and the final length is 10 m. Duration of the hoisting is same as the ramp time $t_{\text{acc}} = 2$ s. Hoisting changes the period of the pendulum from 4.4857 s to 6.3437 s. Other parameters are $s_{\text{ref}} = 10$ s and $v_t = 1$ m/s. The ZV and ZVD shapers use variable delay based on the frequency, i.e. sampling times of the ring buffers are changed during hoisting.

During hoisting movement, pre-computation algorithms keep recalculating ac-

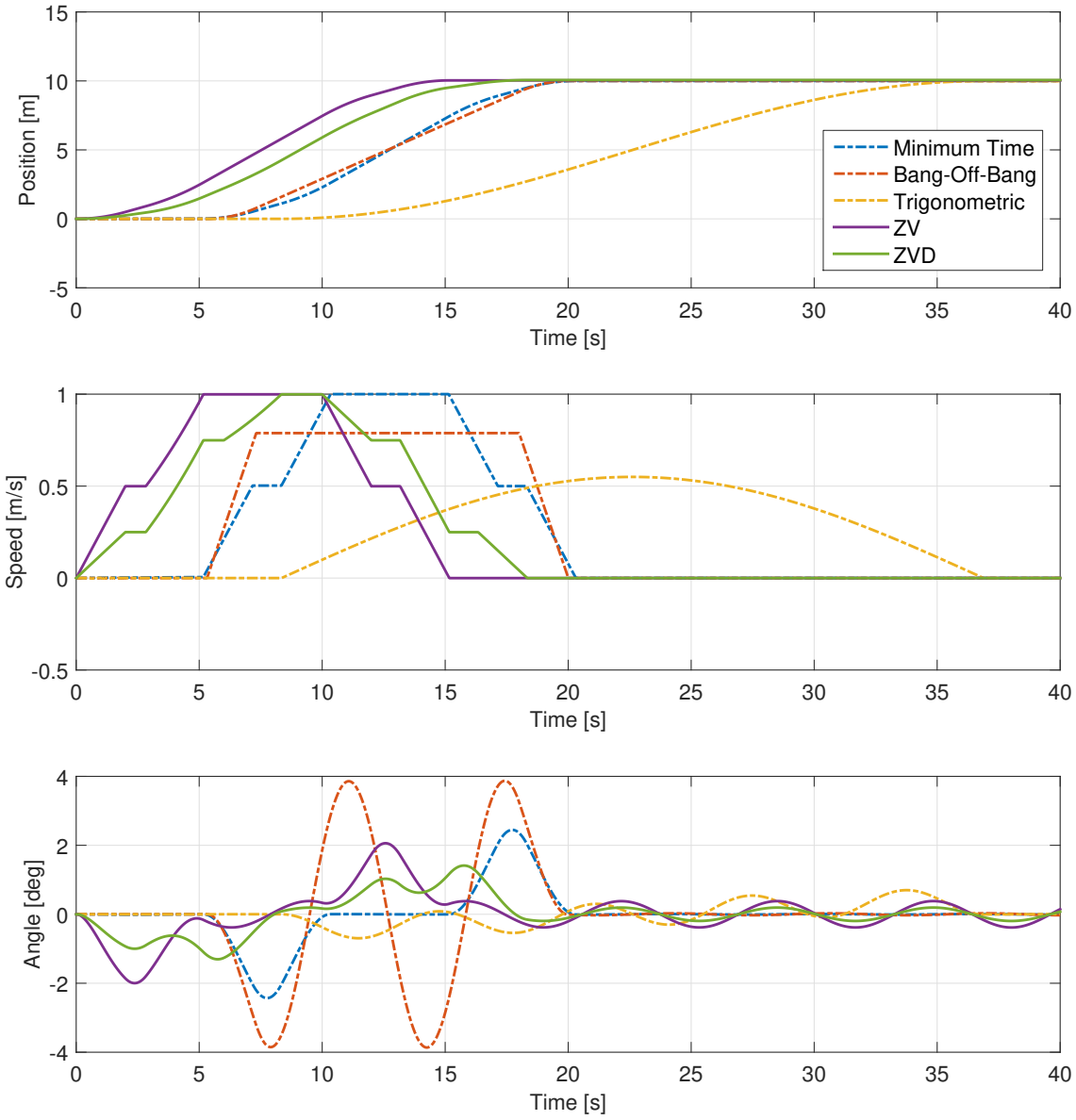

Figure 28: Point-to-point positioning during hoisting movement. The initial rope length is 5 m and the final length is 10 m. Hoisting duration is $t_{\text{acc}} = 2$ s. Other parameters are $s_{\text{ref}} = 10$ s, $v_t = 1$ m/s and $\xi_a = 0$.

celerations. The accelerations are executed at each step cycle, and thus causing a minimal speed and swaying. An initial swaying is compensated after hoisting ends. The sway compensation causes that positioning starts after 5 s, even though hoisting ends at $t = 2$ s. At $t = 5.17$ s, the sway has been compensated and the positioning begins. After positioning there is no residual swaying. Pre-computation algorithms do not leave any residual swaying. Unfortunately, they do not work at all during hoisting and thus making them bad choices. In the worst case, pre-computation algorithms could even decrease productivity when compared to positioning without sway control.

The input shapers work faster than the pre-computation methods, but they leave residual swaying. ZVD is slower than the ZV shaper but it causes less residual swaying. A completely precise model of the crane is not possible and therefore robustness of the input shapers plays an important role.

While hoisting occurs, shaping can also happen at the constant length. Some of the possibilities are shaping at a starting length, an average length or an average frequency [25]. Use of the average length or frequency requires knowledge of how far the payload will be hoisted. Fig. 29a shows residual vibration at different hoisting distance for the ZV shaper. Fig. 29b shows the same for the ZVD shaper. Parameters are the same as in Fig. 28. The residual vibration increases with hoisting distance for all schemes. Shaping at the starting length performs the worst and the residual vibration increases greatly as hoisting distance increases. On the other hand, shaping schemes for the average length and average frequency perform better than shaping at the starting length. Singhose et al. achieved similar results [25]. However, the residual swaying with the variable delay is very minimal which makes it the best choice.

5.3 Simulations Summary

In order to find the most effective point-to-point positioning algorithm, simulation tests were performed. Three of the algorithms used pre-computation and two used input shaping. Pre-computation algorithms were the minimum time strategy, bang-off-bang control and trigonometric shaping. The input shapers were ZV and ZVD shapers.

Pre-computation algorithms were implemented according to the equations presented in the chapter 4 and the sway compensation was integrated into them. The input shapers were implemented with buffers which store values periodically. Positioning algorithm used with the input shapers used trapezoidal or triangular speed curve depending on the situation.

Point-to-point positioning with correct length and zero damping did not pose any problems, as all algorithms reached the end position without swaying and positioning error was nonexistent. A sway during movement depended on how fast the algorithm reached the end position. Therefore, the swaying during movement can be reduced by using small accelerations, even though it leads to a longer positioning time. The bang-off-bang control and trigonometric shaping often have large swaying during movement which can pose a safety risk and stress for crane mechanics. In addition, damping causes problems for pre-computation algorithms because they take damping only into account in the sway tracking. Nevertheless, damping did not cause large oscillations. The input shapers work with damped cranes without problems.

When system parameters are incorrect, performance of the pre-computation algorithms decline rapidly as errors of the system parameters increase. The only exception is the minimum time strategy, as it performed as good as the input shapers. Input shapers can be designed to be robust, so incorrect parameters do not pose large problems for them. An incorrect length is more noteworthy error source than an incorrect damping ratio.

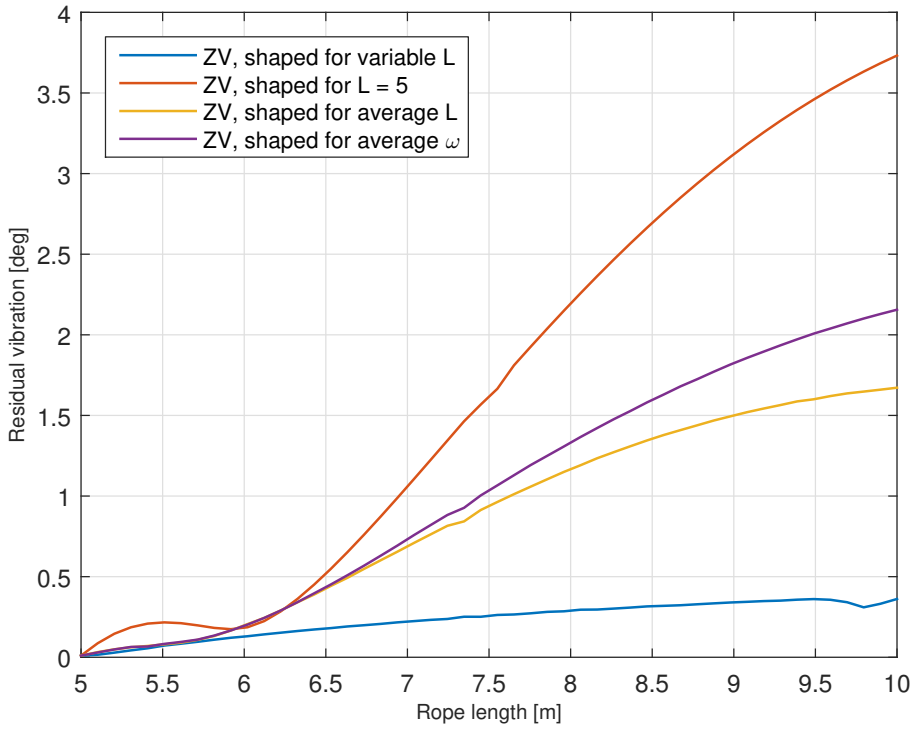

(a) ZV shaper

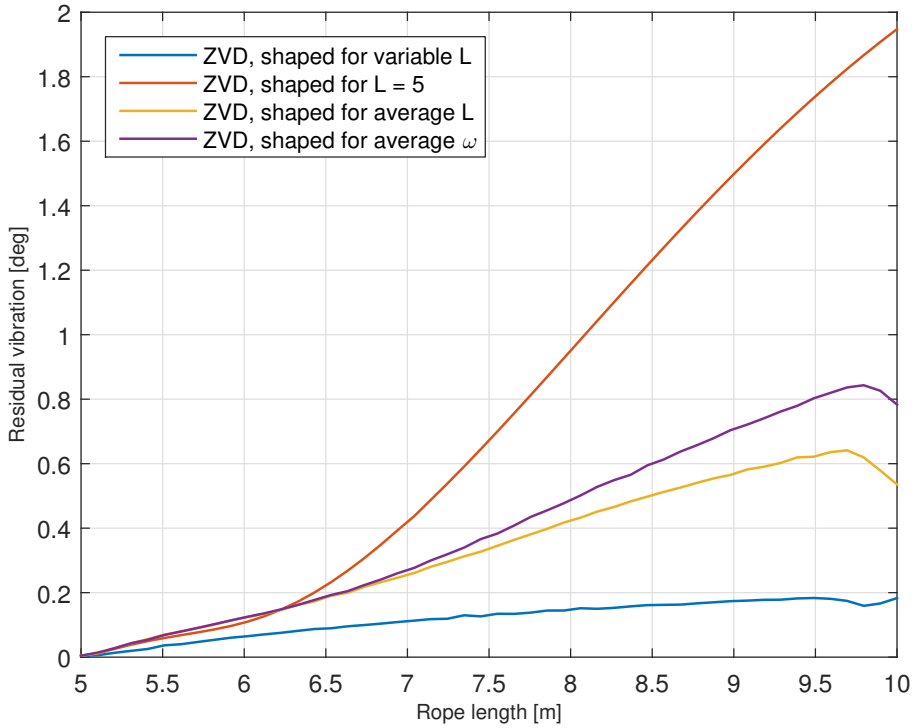

(b) ZVD shaper

Figure 29: The residual vibration at different hoisting distances. The initial length is 5 m and x-axis shows the length after hoisting.

A changing position reference does not cause problems for any of the methods. When the position reference changes, there is an initial speed and swaying. In pre-computation methods, the initial swaying must be compensated before positioning. In contrast, the input shapers do not require similar sway compensation, and consequently can reach the end point faster.

Varying rope length was the most problematic situation. Pre-computation algorithms keep recalculating accelerations during hoisting movement and hence produce very slow results. Nevertheless, they start to work normally when hoisting ends. The pre-computation methods did not leave any residual swaying because the crane model followed the same equations as the sway tracking. However, zero residual swaying does not automatically mean increased productivity. Conversely, the input shapers leave some residual swaying during hoisting. Residual vibration increases with hoisting distance. The ZVD shaper is robuster than the ZV shaper and hence worked better. The least swaying is achieved when the buffers of the shapers use variable delay time. Although the ZVD shaper could not remove all residual swaying in this last test, overall it outperformed other methods.

6 Hardware Tests

The algorithms were compared in the previous chapter. As a result, a ZVD shaper was chosen as the most effective positioning algorithm. Performance of the ZVD shaper was tested using a real overhead crane in China. This chapter presents the test setup and positioning results.

6.1 Test Setup

A block diagram of the test setup is presented in Fig. 30. The crane could lift 10 tons and the test load was 6 tons. Motors rotate wheels and hoisting drum of the crane and they are controlled with variable-speed drives. There are three drives which control hoisting, trolley and long travel movements. The test setup used position feedback. The programmable logic controller (PLC) sends a position reference and a position feedback to drive. The actual speed of the motor is measured with a high transistor logic (HTL) encoder, which is sent to the PLC via a wired Profinet connection. The used PLC was Siemens S7-1500. However, the test setup did not include sway measurement and swaying was estimated only by eyesight.

The positioning algorithm used shaping of a position reference and it was implemented into the variable-speed drive. Shaping of the position reference is described in the section 4.3. The cycle time of the program was 6 ms. Fig. 31 shows the block diagram for the positioning blocks and position control. The signal from PLC was discontinuous and hence additional low pass filters were added. Filter after the ZVD shaper had a filter time constant of 50 ms. On the other hand, other filters had the filter time constants of 100 ms. The ZVD shaper was implemented using an identical algorithm as used in the simulations. An interpolator (IPO) created a position profile from a step reference.

IPO shaped a step position reference into a s-curve. IPO has four parameters: position reference, maximum speed, positioning acceleration and positioning deceleration. The positioning acceleration and deceleration are identical and they used values from the crane technical specification. Output of the interpolator, which is a s-curve, is created by accelerating to a speed limit which varies at the traveled distance. The speed limit is

$$v_{\text{lim}} = \sqrt{2(s_{\text{ref}} - s_{\text{act}})a_{\text{dec}}} \tag{88}$$

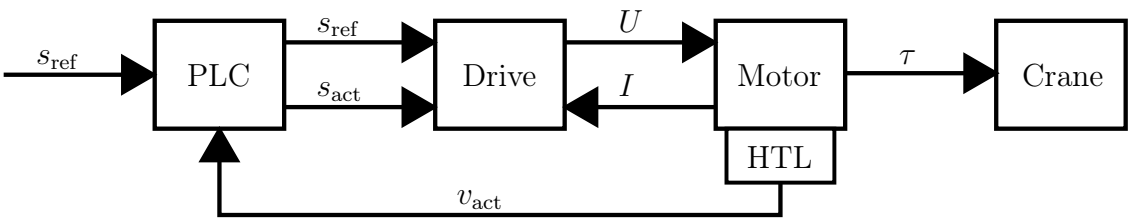

Figure 30: Block diagram of the test setup. s_{ref} is the position reference, s_{act} is the measured actual position, v_{act} is the measured actual speed, I is the motor current, U is the motor voltage and τ is the torque.

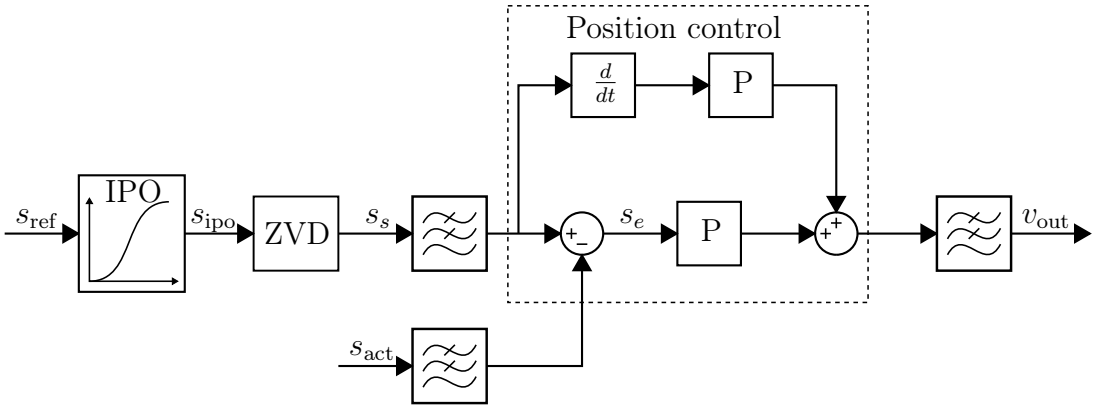

Figure 31: Block diagram for positioning blocks and position control used in the hardware tests. s_{ref} is the position reference, s_{ipo} is the position profile, s_s is the shaped position reference, s_{act} is the measured actual position, s_e is the position error and v_{out} is the output speed.

where s_{ref} is the reference position, s_{act} is the actual position and a_{dec} is the positioning deceleration. S-curve is achieved by using either a trapezoidal or triangular speed profile. Phases of the speed profile are acceleration, constant speed phase and deceleration. The first phase is acceleration to the speed limit. Speed stays constant as long as the speed limit is over the maximum velocity. The deceleration phase begins when the speed limit decreases below the maximum velocity. The speed limit cannot be larger than the maximum velocity which was 107 m/min for the long travel motion. Code of the basic IPO functionality is presented in the appendix B.

6.2 Positioning Tests

Positioning was tested using both long travel and trolley drives. Figs. 32 and 33 show filtered encoder speed, position feedback, anti-sway position output, positioning speed reference and position reference s_{ref}. The position feedback is the same as the actual position s_{act}, the anti-sway position output is the same as the shaped position reference s_s and the positioning speed reference is the same as the output speed v_{out}. The filtered encoder speed has a filter time constant of 3 ms. The ZVD shaper required the length of the rope which was calculated. The calculated length was 7.35 m. The real length of the rope was not measured.

Fig. 32 shows positioning to from an initial position of 9.6 m to 35 m. Positioning took approximately 30 seconds. According to the monitor file, positioning accuracy is 1 mm. Fig. 33 shows positioning from 35 m to 5 m. This test also had positioning accuracy of 1 mm. Precise positioning requires feedback as the shaped position reference and position feedback are not identical. Without feedback, excellent positioning accuracy is hard to achieve. Therefore, open-loop positioning suits only for applications, in which positioning accuracy is not the highest priority. Positioning accuracy is based on monitor values and in reality, accuracy may be less.

Some of the test scenarios were recorded with a video camera. The swaying of the payload is very minimal and it is hard to notice. According to the hardware

tests, the ZVD shaper can remove swaying of the payload and the target position is reached. Achieved positioning accuracy is good, when feedback is used, and residual swaying is nonexistent.

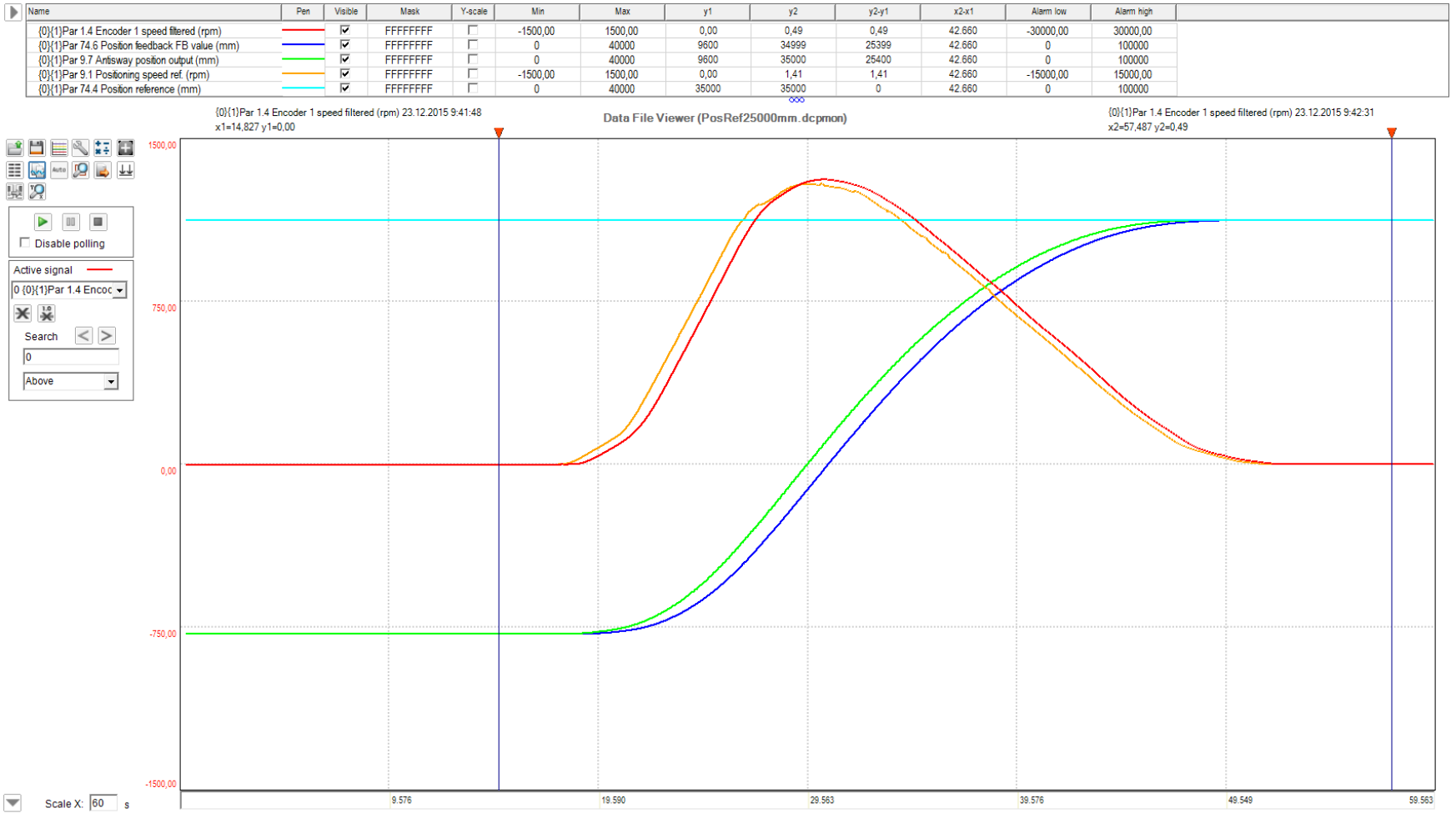

Figure 32: Positioning from 9.6 m to 35 m.

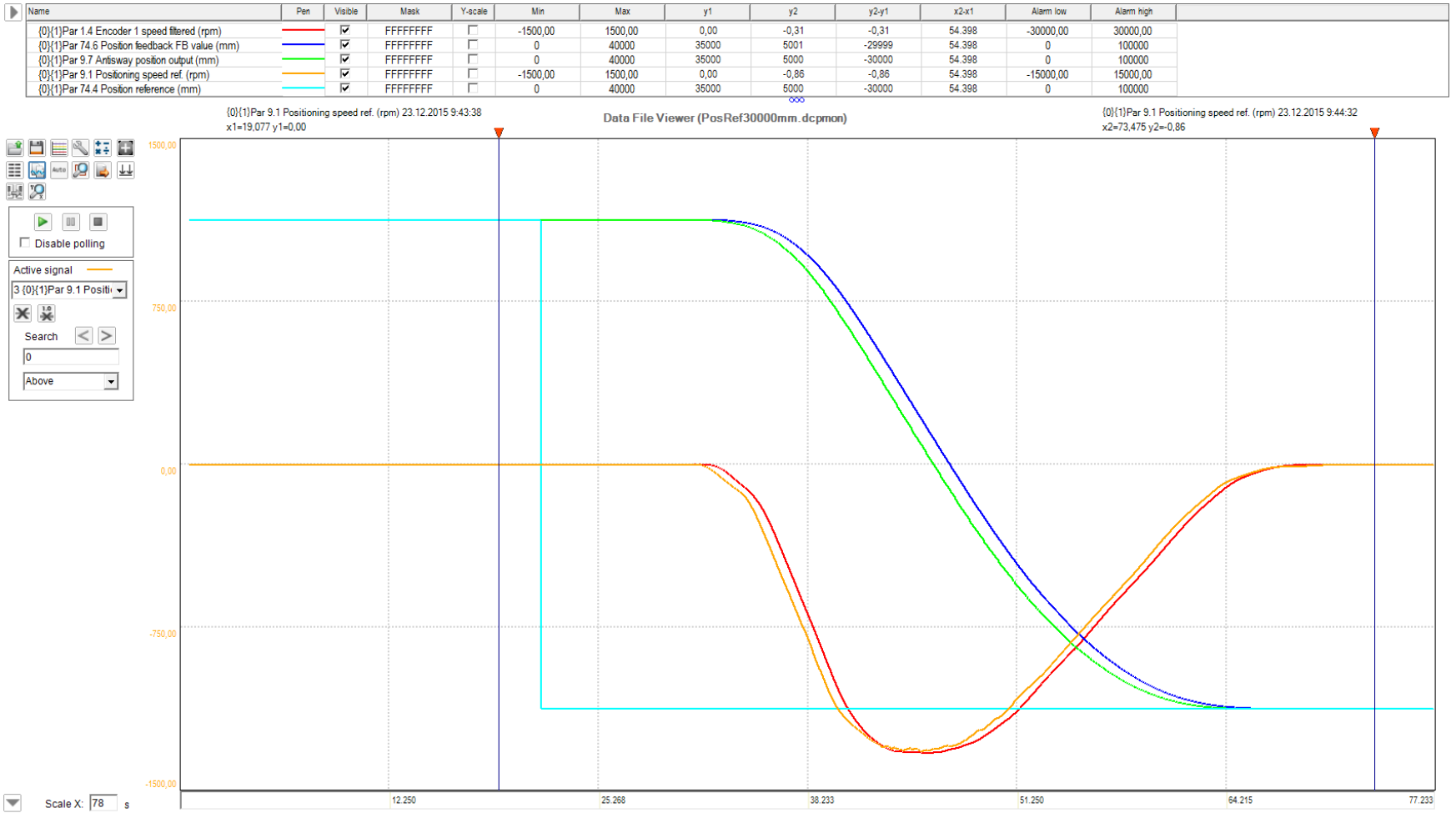

Figure 33: Positioning from 35 m to 5 m.

7 Summary

In this thesis, positioning algorithms were developed in order to position a crane without swaying of a payload. These positioning algorithms used command shaping, in which a reference signal is modified. Three of the algorithms were implemented using pre-computed command profiles and two of the algorithms used one type of real-time command shaping technique, referred to as input shaping. Pre-computed commands profiles might feel more intuitive approach, as the whole motion profile is calculated when a reference is given. Input shaping delays parts of the reference signal in order to suppress payload oscillations.

Performance of the algorithms was tested using Simulink simulations. As a result, all algorithms managed to reach the position reference and positioning error was nonexistent in all test cases. However, pre-computation algorithms can not diminish effects of damping and they are more susceptible to errors of system parameters than input shapers, what leads to oscillations. In addition, pre-computation schemes produce very slow results when positioning during hoisting. In many situations, the input shapers were the superior choice. The used input shapers were ZV and ZVD shapers. However, the only problematic situation for the input shapers is positioning during hoisting, in which the input shapers do not remove all oscillations. Nevertheless, oscillations are greatly reduced. The ZV shaper is faster than the ZVD shaper, although extra robustness of the ZVD shaper is a great asset. Robustness is an important trait, as a perfect model of a crane is impossible to implement. Therefore, crane parameters always have more or less inaccuracy. Increased robustness of shapers generally has one drawback: increased rise time. Whether increased robustness is worth the longer ramp times depends on the situation. Overall, the ZVD shaper is the better choice than the ZV shaper.

In addition, positioning was tested using a real overhead crane, in which the positioning algorithm used a ZVD shaper. The ZVD shaper was used for shaping of a position reference. The test setup contained a position feedback, which improved positioning accuracy. As a result, positioning accuracy was good and the ZVD shaper managed to remove payload oscillations. Positioning requires feedback if positioning accuracy is priority. On the other hand, open-loop positioning suits well for indoor applications, in which positioning accuracy is not extremely important. This thesis succeeded in creating a positioning algorithm which is suitable for example waste handling and transport.

The future research could investigate sensor technology, as the open-loop sway control can not remove the effects of external disturbances. Another future research option could be performance of warehouse lifts using input shaping, as they start to oscillate from the top during movement. Physically, a warehouse lift and overhead crane follow almost identical equations.

References

[1] K. L. Sorensen, W. Singhose, and S. Dickerson, "A Controller Enabling Precise Positioning and Sway Reduction in Bridge and Gantry Cranes," *Control Eng. Practice*, vol. 15, no. 7, pp. 825-837, Jul. 2007.

[2] M. A. Ahmad, A. N. K. Nasir, and H. Ishak, "Techniques of anti-sway and input tracking control of a gantry crane system," *2009 IEEE Int. Conference on Mechatronics and Automation*, Vol. 5246357, pp. 262-267, Aug. 2009

[3] W. E. Singhose, "Command Generation for Flexible Systems," Ph.D. dissertation, Dept. Mech. Eng., MIT, Cambridge, 1997.

[4] B. H. Karnopp, "A Strategy for Moving a Mass from One Point to Another," *J. of the Franklin Inst.*, Vol. 329, no. 5, pp. 881-892, Sep. 1992.

[5] P. Dadone, and H. F. Vanlandingham, "Load Transfer Control for a Gantry Crane with Arbritrary Delay Constraits," *J. of Vibration and Control*, vol. 8, no. 2, pp. 135-158, Feb. 2002.

[6] H. M. Omar, "Control of Gantry and Tower Cranes," Ph.D. dissertation, Dept. Mech. Eng., Virginia Tech, Blacksburg, 2003.

[7] L. D. Landau, and E. M. Lifshitz, "Equations of Motion," in *Mechanics*, 3rd ed. Oxford, United Kingdom: Butterworth-Heinemann, 1976.

[8] K. L. Sorensen, "A Combined Feedback and Command Shaping Controller for Improving Positioning and Reducing Cable Sway in Cranes," M.Sc. Thesis, Dept. Mech. Eng, Georgia Tech, Atlanta, 2005.

[9] J. Pitkäranta, "Differentiaaliyhtälöt," in *TKK:n Laaja matematiikka 2.* Helsinki, Finland: Edita Prima, 2007, pp. 603-686.

[10] J. Pitkäranta, "Taylorin sarjat," in *TKK:n Laaja matematiikka 1.* Helsinki, Finland: Edita Prima, 2009, pp. 406-472.

[11] O. Mård, and R. Ahvo, "Method for Damping the Load Swing of a Crane," U.S Patent 5 799 805, 9.1.1998.

[12] R. Salminen, "Robust Pole Placement Control of a Trolley Crane System," Ph.D dissertation, Autom. Tech. Lab, Helsinki Univ. of Technology, Espoo, Finland, 1992.

[13] K. Hytönen, "Siltanosturin Dynaaminen Ohjaus," M.Sc: Thesis, Dept. Process. Eng, Univ. of Oulu, Oulu, 1989.

[14] G. P. Starr, "Swing-free Transport of Suspended Objects with a Robot Manipulator," *J. of Dynamic Systems, Measurements and Control*, Transactions of the ASME, vol. 107, no. 1, pp. 97-100, Mar. 1985.

[15] W. Singhose, "Command Shaping for Flexible Systems: a Review of the First 50 Years," *Int. J. of Precision and Manufacturing*, vol. 10, no. 4, pp. 153-168, Oct. 2009.

[16] J. Fortgang, "Concurrent Design of Input Shaping and Vibration Absorbers," M.Sc. Thesis, Dept. Mech. Eng, Georgia Tech, Atlanta, 2001.

[17] W. E. Singhose, L. J. Porter, and W. P. Seering, "Input Shaped Control of a Planar Gantry Crane with Hoisting," *Proc. of the Amer. Control Conference*, vol. 1, pp. 97-100, Jun. 1997.

[18] N. C. Singer, and W. P. Seering, "Preshaping Command Inputs to Reduce System Vibration," *J. of Dynamic Syst., Measurement and Control, Trans. of the ASME*, Vol 112, no. 1, pp. 76-82, Mar. 1990.

[19] T. Singh, and W. Singhose, "Tutorial on Input Shaping/Time Delay Control on Maneuvering Flexible Structures," *Proc. of the Amer. Control Conference*, vol. 3, pp. 1717-1731, 2002.

[20] J. Vaughan, A. Yano, and W. Singhose, "Comparison of robust input shapers," *J. of Sound and Vibration*, vol. 315, no. 4-5, pp. 797-815, Sep. 2008.

[21] ABB Drives, "Crane Control and Safety with the ACS880 Industrial Drives," 2015. [Online]. Available: https://library.e.abb.com/public/9f4ec89f17334805938b6851896a5119/Crane_control_and_safety_with_the_ACS880_industrial_drives.pdf

[22] E. M. Abdel-Rahman, A.H. Nayfeh, and Z.N. Masoud, "Dynamics and Control of Crane: a Review," *J. of Vibration and Control*, vol. 9, no. 7, pp. 863-908, Jul. 2003.

[23] J. J. Hämäläinen, A. Marttinen, L. Baharova, and J. Virkkunen, "Optimal Path Planning for a Trolley Crane: Fast and Smooth Transfer of Load," *IEE Proc.: Control Theory and Applications*, vol. 142, no. 1, pp. 51-57, Jan. 1995.

[24] H. D. Young, and R.A. Freedman, "Motion along a straight line," in *University Physics with Modern Physics*, 12th ed. San Francisco, USA: Pearson Addison-Wesley, 2008, pp. 36-60.

[25] W. Singhose, L. Porter, M. Kenison and E. Kriikku, "Effects of Hoisting on the Input Shaping Control of Gantry Cranes." *Control Eng. Practice*, vol. 8, no. 10, pp. 1159-1165, Oct. 2000.

[26] N. S. Singer, "Residual Vibration Reduction in Computer Controlled Machines," Ph.D. dissertation, Dept. Mech. Eng, MIT, Cambridge, 1988.

A Derivation of ZVD Equations

A ZVD shaper has a one additional constraint compared to a ZV shaper, which is

$$\frac{\partial}{\partial \omega_n} V(\omega_n, \xi) = 0 \tag{A1}$$

Due to Eq. (A1) two new equations are added to the system:

$$\frac{\partial}{\partial \omega_n} C = \frac{\partial}{\partial \omega_n} \sum_{i=1}^{N} A_i e^{\xi \omega_n t_i} \cos\left(\omega_n \sqrt{1-\xi^2} t_i\right) = 0 \tag{A2}$$

$$\frac{\partial}{\partial \omega_n} S = \frac{\partial}{\partial \omega_n} \sum_{i=1}^{N} A_i e^{\xi \omega_n t_i} \sin\left(\omega_n \sqrt{1-\xi^2} t_i\right) = 0 \tag{A3}$$

Deriving C and S gives us

$$0 = \sum_{i=1}^{N} \left[A_i t_i \sqrt{1-\xi^2} e^{\xi \omega_n (t_N - t_i)} \cos\left(\omega_n \sqrt{1-\xi^2} t_i\right) - A_i \xi (t_N - t_i) e^{\xi \omega_n (t_N - t_i)} \sin\left(\omega_n \sqrt{1-\xi^2} t_i\right) \right] \tag{A4}$$

$$0 = \sum_{i=1}^{N} \left[-A_i t_i \sqrt{1-\xi^2} e^{\xi \omega_n (t_N - t_i)} \sin\left(\omega_n \sqrt{1-\xi^2} t_i\right) - A_i \xi (t_N - t_i) e^{\xi \omega_n (t_N - t_i)} \cos\left(\omega_n \sqrt{1-\xi^2} t_i\right) \right] \tag{A5}$$

Next both sides are divided with $\sqrt{1-\xi^2}$ and it is assumed that second term in Eqs. (A4) and (A5) is zero. It is shown below that the assumption is valid. Result is then

$$\sum_{i=1}^{N} A_i t_i e^{\xi \omega_n (t_N - t_i)} \cos\left(\omega_n \sqrt{1-\xi^2} t_i\right) = 0 \tag{A6}$$

$$\sum_{i=1}^{N} A_i t_i e^{\xi \omega_n (t_N - t_i)} \sin\left(\omega_n \sqrt{1-\xi^2} t_i\right) = 0 \tag{A7}$$

Now it is shown that, if (A6) is true, the second term in the Eq. (A4) is equal to zero. The second term of Eq. (A6) divided with $\sqrt{1-\xi^2}$ is

$$\frac{A_i \xi (t_N - t_i) e^{\xi \omega_n (t_N - t_i)} \sin\left(\omega_n \sqrt{1-\xi^2} t_i\right)}{\sqrt{1-\xi^2}} = \frac{A_i \xi t_N e^{\xi \omega_n (t_N - t_i)} \sin\left(\omega_n \sqrt{1-\xi^2} t_i\right)}{\sqrt{1-\xi^2}} - \frac{A_i \xi t_i e^{\xi \omega_n (t_N - t_i)} \sin\left(\omega_n \sqrt{1-\xi^2} t_i\right)}{\sqrt{1-\xi^2}} \tag{A8}$$

Eq. (A8) can be rearranged to make it more clear:

$$\frac{A_i \xi (t_N - t_i) e^{\xi \omega_n (t_N - t_i)} \sin\left(\omega_n \sqrt{1-\xi^2} t_i\right)}{\sqrt{1-\xi^2}} = \frac{\xi t_N}{\sqrt{1-\xi^2}} A_i e^{\xi \omega_n (t_N - t_i)} \sin\left(\omega_n \sqrt{1-\xi^2} t_i\right) - \frac{\xi}{\sqrt{1-\xi^2}} A_i t_i e^{\xi \omega_n (t_N - t_i)} \sin\left(\omega_n \sqrt{1-\xi^2} t_i\right) \tag{A9}$$

Other two constraints of the ZVD shaper are

$$C(\omega_n, \xi) = \sum_{i=1}^{N} A_i e^{\xi\omega_n t_i} \cos\left(\omega_n\sqrt{1-\xi^2}t_i\right) = 0 \tag{A10}$$

$$S(\omega_n, \xi) = \sum_{i=1}^{N} A_i e^{\xi\omega_n t_i} \sin\left(\omega_n\sqrt{1-\xi^2}t_i\right) = 0 \tag{A11}$$

The first term in Eq. (A9) has same expression as (A10), which makes it zero. Term that is left has exactly the same expression as (A6). Therefore the second term in Eq. (A4) is zero. Same thing applies for S. [26]

Time location of the first impulse can be set to zero. Now unknowns of the ZVD shaper can be solved from the following system of equations:

$$\begin{cases} \sum_{i=1}^{N} A_i e^{\xi\omega_n t_i} \cos\left(\omega_n\sqrt{1-\xi^2}t_i\right) = 0 & \text{(A12)} \\ \sum_{i=1}^{N} A_i e^{\xi\omega_n t_i} \sin\left(\omega_n\sqrt{1-\xi^2}t_i\right) = 0 & \text{(A13)} \\ \sum_{i=1}^{N} A_i t_i e^{\xi\omega_n (t_N - t_i)} \cos\left(\omega_n\sqrt{1-\xi^2}t_i\right) = 0 & \text{(A14)} \\ \sum_{i=1}^{N} A_i t_i e^{\xi\omega_n (t_N - t_i)} \sin\left(\omega_n\sqrt{1-\xi^2}t_i\right) = 0 & \text{(A15)} \\ \sum_{i=1}^{N} A_i = 1 & \text{(A16)} \end{cases}$$

Rest of the derivation is just mechanical solving as in derivation of the ZV shaper. The ZVD shaper has three impulses and result is

$$\begin{bmatrix} A_1 & A_2 & A_3 \\ t_1 & t_2 & t_3 \end{bmatrix} = \begin{bmatrix} \frac{1}{1+2K+K^2} & \frac{2K}{1+2K+K^2} & \frac{K^2}{1+2K+K^2} \\ 0 & 0.5T_d & T_d \end{bmatrix} \tag{A17}$$

where $K = e^{-\frac{\xi\pi}{\sqrt{1-\xi^2}}}$.

B Interpolator Code

Interpolator has four parameters: positioning acceleration, position deceleration and positioning speed. Parameter *time* is steptime of the Simulink. Basic functionality of IPO can be represented in Matlab code as follows:

```
1 function PosOut  = fcn(PosRef, Acc, Dec, v_max, time)
2
3   persistent PosIPOOut ActIPOSpeed
4
```

```
5    % initialize persistent variables
6    if isempty(ActIPOSpeed)
7        ActIPOSpeed = 0;
8        PosIPOOut = 0;
9    end
10
11   % direction
12   DisToTarget = PosIPOIn - PosIPOOut;
13
14   % calculate speed limit
15   v_lim = sqrt(2*abs(DisToTarget)*Dec);
16   v_lim = v_lim - Dec/2*time;
17   if v_lim < Dec/2*time
18       v_lim = abs(DisToTarget)/time;
19   end
20
21   if v_lim > v_max
22       v_lim = v_max;
23   end
24
25   % increment or decrement speed
26   if sign(DisToTarget) < 0
27       v_lim = -v_lim;
28       if ActIPOSpeed > 0
29           ActIPOSpeed = ActIPOSpeed - Dec*time;
30       elseif (ActIPOSpeed - Acc*time) > v_lim
31                ActIPOSpeed = ActIPOSpeed - Acc*time;
32       else
33           ActIPOSpeed = ActIPOSpeed + Dec*time;
34           if ActIPOSpeed > v_lim
35               ActIPOSpeed = v_lim;
36           end
37       end
38   else
39       if ActIPOSpeed < 0
40           ActIPOSpeed = ActIPOSpeed + Dec*time;
41       elseif (ActIPOSpeed + Acc*time) < v_lim
42                ActIPOSpeed = ActIPOSpeed + Acc*time;
43       else
44           ActIPOSpeed = ActIPOSpeed - Dec*time;
45           if ActIPOSpeed < v_lim
46               ActIPOSpeed = v_lim;
47           end
48       end
49   end
50
51   % update position
52   PosIPOOut = PosIPOOut + ActIPOSpeed*time;
53   PosOut = PosIPOOut;
54 end
```